Systems/Circuits

Optogenetic Activation of V1 Interneurons Reveals the Multimodality of Spinal Locomotor Networks in the Neonatal Mouse

Melanie Falgairolle and Michael J. O'Donovan
Developmental Neurobiology Section, National Institute of Neurological Disorders and Stroke, National Institutes of Health, Bethesda, Maryland 20892

In the spinal cord, classes of interneurons have been studied *in vitro* to determine their role in producing or regulating locomotion. It is unclear whether all locomotor behaviors are produced by the same circuitry or engage different subsets of neurons. Here, in neonatal mice of either sex, we test this idea by comparing the actions of a class of spinal, inhibitory interneuron (V1) expressing channelrhodopsin driven by the *engrailed-1* transcription factor on the rhythms elicited by different methods. We find that, although the overall locomotor activities *in vitro* are similar, V1 interneuron depolarization produces opposite effects depending of the mode of activation of the locomotor circuitry. The differential behavior of V1 neurons suggests that their function depends on how the locomotor rhythm is activated and is consistent with the idea that the functional organization of the corresponding locomotor networks also differs.

Key words: **central pattern generator; Engrailed-1; locomotion; optogenetic; spinal cord; V1**

Significance Statement

The neural networks dictating the execution of fictive locomotion are located in the spinal cord. It is generally assumed that the mode of activation of these spinal networks should not change the recruitment or function of neurons. Here, we manipulated the activity of a class of interneuron (V1), which targets these networks and found that their activation induces opposite effects depending on the mode of activation. This suggests that the mode of activation of the spinal networks differentially recruits either V1 interneurons or other interneurons, or both.

Introduction

In the isolated spinal cord of the neonatal rodent, fictive locomotion can be initiated by drugs, by dorsal or ventral root stimulation, or by stimulation of descending brainstem pathways (Zaporozhets et al., 2004; Mentis et al., 2005; Pujala et al., 2016; Whelan et al., 2000). In the neonatal mouse, locomotor-like activity evoked by sacrocaudal afferents or by a drug cocktail generates an average duty cycle that is larger in extensor compared with flexor ventral roots (Falgairolle and O'Donovan, 2019). During brainstem stimulation, the relationship reverses and the duty cycle of the flexor ventral roots is the longest (this paper), similar to what has been described in the adult cat (Yakovenko et al., 2005; Frigon and Gossard, 2009). In addition, in the adult cat, in successive episodes of treadmill locomotion, only 20% of the neurons are common to both episodes (Pham et al., 2020). These last results indicate a surprising degree of flexibility in the networks responsible for locomotion and challenge the idea that a fixed network is responsible for generating the various forms of locomotion. Moreover, work in the mouse has shown that the neurons active in the central pattern generator (CPG) change with the speed of locomotion (Crone et al., 2009; Rancic et al., 2020). One approach to this problem is to examine the function of a genetically identified neuronal class to establish whether it differs according to the type of locomotion and how it is initiated. For this purpose, we use optogenetics to examine the function of V1 interneurons under the different conditions. V1 interneurons are inhibitory, ipsilaterally projecting neurons that express the transcription factor *Engrailed-1* (*En1*). They have been implicated in regulating the frequency of the locomotor rhythm in mice and zebrafish both *in vivo* and *in vitro* (Gosgnach et al., 2006; Britz et al., 2015; Falgairolle and O'Donovan, 2019; Kimura and Higashijima, 2019), using either optogenetic or chemogenetic methods to hyperpolarize the V1 population (Gosgnach et al., 2006; Falgairolle and O'Donovan,

Received Apr. 23, 2021; revised July 16, 2021; accepted Aug. 17, 2021.

Author contributions: M.F. and M.J.O. designed research; M.F. performed research; M.F. analyzed data; M.F. and M.J.O. wrote the first draft of the paper; M.F. and M.J.O. edited the paper; M.F. and M.J.O. wrote the paper.

This research was supported by the Intramural Research Program of the National Institutes of Health, National Institute of Neurological Disorders and Stroke.

The authors declare no competing financial interests.

Correspondence should be addressed to Melanie Falgairolle at melanie.falgairolle@nih.gov.

https://doi.org/10.1523/JNEUROSCI.0875-21.2021

Copyright © 2021 the authors

2019), or genetic methods to functionally delete the neurons or their synaptic effects (Gosgnach et al., 2006; Britz et al., 2015; Kimura and Higashijima, 2019). In the zebrafish, it was shown that V1s are responsible for the emergence of fast rhythmic behavior by suppressing the spinal circuitry that produces slow swimming and inhibiting motoneurons (MNs) to shorten their burst duration (Kimura and Higashijima, 2019). In mammalian networks, their function is more complex because they control both the pattern and the frequency of the rhythm. Their outputs vary according to the function of MNs they innervate (Bikoff et al., 2016; Sweeney et al., 2018), with a greater projection to flexor compared with extensor MNs (Britz et al., 2015). Consistent with the data in the zebrafish, when V1 neurons are inhibited in the neonatal mouse, the frequency of fictive locomotion is reduced and this effect is frequency-dependent during drug-induced locomotion (Falgairolle and O'Donovan, 2019).

In the present work, we tested whether V1 depolarization has similar actions according to how fictive locomotion was produced. To do so, we expressed Channelrhodopsin-2 (ChR2), a sodium channel that depolarizes neurons when exposed to blue light into V1 interneurons. We verified that the expression was specific and that the global effect of V1 depolarization was inhibitory. In the whole cord and hemicord, their depolarization slows the rhythm. By contrast, during brainstem stimulation, V1 depolarization accelerates the rhythm but causes little change during sacral afferent-evoked fictive locomotion. The light-induced frequency changes were more pronounced in preparations with faster locomotor rhythms. These findings suggest that the function of V1s during locomotor activity depends not only on the type of locomotion, but also on how the rhythm is activated, and support the idea that the organization of locomotor CPGs is less rigid than generally assumed.

Materials and Methods

Animals. All experiments were conducted in compliance with the National Institute of Neurologic Disorders and Stroke Animal Care and Use Committee (Animal Protocol Number 1267).

Experiments were performed on Swiss Webster WT (Taconic Laboratory) or transgenic mice between the day of birth to postnatal day 5 (P0-P5) of either sex. We used several different transgenic mouse lines in the experiments: ChR2-EYFP (ChR2, B6;Cg-*Gt[ROSA]26Sor*$^{tm32[CAG-COP4*H134R/EYFP]Hze}$/J, stock #024109), Arch-GFP (Arch, B6;129S-*Gt[ROSA]26Sor*$^{tm35.1[CAG-aop3/GPF]Hze}$/J, stock #012735), floxed EGFP (EGFP, *Gt[ROSA]26Sor*$^{tm1.1[CAG-EGFP]Fsh}$/Mmjax, MMRRC stock #32 037-JAX), and floxed tdT (tdT, B6.Cg-*Gt[ROSA]26Sor*$^{tm9[CAG-tdTomato]Hze}$/J, stock #007909) were obtained from Jackson ImmunoResearch Laboratories, whereas *En1*-cre was kindly gifted by Martyn Goulding.

Dissection. After decapitation, mice were eviscerated and subsequently transferred to a dissecting chamber continuously superfused with aCSF (concentrations in mM as follows: 128.35 NaCl, 4 KCl, 1.5 $CaCl_2.H_2O$, 1 $MgSO_4{\cdot}7H_2O$, 0.58 $NaH_2PO_4{\cdot}H_2O$, 21 $NaHCO_3$, 30 D-glucose) and bubbled with 95% O_2 and 5% CO_2. After a ventral laminectomy, the cords were isolated together with the attached roots and ganglia and left at room temperature. For experiments with the brainstem attached, mice were first anesthetized with isoflurane, and the cord was isolated as described above but with the brainstem attached. For experiments with intracellular recordings, the pia was removed on the ventral or the lateral part of the left L5 segment. In some preparations, we removed the dorsal pia on the lumbar segments and pinned down the spinal cord dorsal up onto a strip of beeswax that was mounted on a small piece of Plexiglas. The cords were then transferred to a vibratome chamber containing an ice slush, oxygenated low calcium, high magnesium aCSF (28.35 NaCl, 4 KCl, 0.5 $CaCl_2{\cdot}H_2O$, 6 $MgSO_4.7H_2O$, 0.58 $NaH_2PO_4{\cdot}H_2O$, 21 $NaHCO_3$, 30 D-glucose) or a K-gluconate–based solution (concentrations in mM as follows: 130 K-gluconate, 15 KCl, 0.05 EGTA, 20 HEPES, 25 D-glucose, 1 mM kynurenic acid, 2 mM Na-pyruvate, adjusted to pH 7.4 with KOH). The dorsal part of the lumbar spinal cord (~250 μM, or until the central canal was visible) was then removed with a razor blade mounted on the vibratome. The cord was then transferred to a recording chamber with aCSF at room temperature and allowed to recover for at least 30 min.

Electrophysiological recordings. MN extracellular activity was recorded using tight-fitting plastic suction electrodes. Recordings were obtained from three lumbar ventral roots: two from the flexor-dominated ventral roots (either L1 or L2: left and right) and one from an extensor-dominated ventral root (L5: left or right). Fictive locomotion was elicited in three different ways: (1) using a drug cocktail: NMDA (5 μM), serotonin creatinine sulfate monohydrate (5-HT, 10 μM), and dopamine (DA, 50 μM); (2) stimulation of a sacral DRG or a sacral dorsal root (4 Hz, train duration: 10 s, stimulus duration: 250 μs); or (3) by stimulating the brainstem (4 Hz, train duration: 20 s, stimulus duration: 250 μs) using a bipolar electrode placed on the ventromedial medulla (Zaporozhets et al., 2004; Pujala et al., 2016). Strychnine (5 μM), a glycine receptor antagonist, and bicuculline (20 μM), a GABA receptor antagonist, were used in some experiments to produce rhythmic bursting (Bracci et al., 1996).

In all experiments, the signals were amplified (1000 times), bandpass filtered between 0.1 Hz and 3 kHz, and digitized at 10 kHz (Digidata 1322A, 1440A, 1500; Molecular Devices) and stored for further analysis. NMDA, 5-HT, DA, strychnine, and bicuculline were obtained from Sigma-Aldrich.

Intracellular recordings. Whole-cell recordings were obtained from MNs or interneurons with patch electrodes pulled from borosilicate capillaries with a microelectrode puller (model P-80 or P-97, Sutter Instruments). To perform blind-patching, after removing the pia matter, pipettes (resistance: 3-11 MΩ) were advanced into the ventral horn of the spinal cord. Patch electrodes were filled with an intracellular solution containing 10 mM NaCl, 130 mM K-gluconate, 10 mM HEPES, 11 mM EGTA, 1 mM $MgCl_2$, 0.1 mM $CaCl_2$, and 1 mM Na_2ATP (pH adjusted to 7.2-7.4 with KOH). For some experiments, 5 mM QX-314 and 5 mM cesium were added to the intracellular solution to allow the measurement of synaptic currents and/or the photocurrents generated by activation of V1s. In another set of experiments, using *En1*-tdT-Arch animals, the dorsal part of the lumbar spinal cord was removed to gain access to ventrally located interneurons. Interneurons were then visually targeted with glass pipettes (resistance: 3-4 MΩ) filled with an intracellular solution containing 10 mM NaCl, 130 mM K-gluconate, 10 mM HEPES, 11 mM EGTA, 1 mM $MgCl_2$, 0.1 mM $CaCl_2$, and 1 mM Na_2ATP, and Alexa-350 hydrazide 50 μM (pH adjusted to 7.2-7.4 with KOH). Neurons were only considered for subsequent analysis if they exhibited a stable resting membrane potential and, for MNs, if they exhibited an overshooting antidromically evoked action potential. The input resistance was calculated from the slope of the current/voltage (200 ms) plot within the linear range. The liquid junction potential was not corrected. All recordings were obtained with a Multiclamp 700A or 700B (DC-3kHz, Molecular Devices).

Activation of the opsins. To activate ChR2, we illuminated the cord ventrally with a train (1 ms at 100 Hz) of blue light (415-475 nM); whereas to activate Arch, continuous light (540-600 nm) was used (light-emitting diode, X-cite, Excelitas). To illuminate the whole lumbar cord, we used a 3-mm-diameter light guide. The maximum light intensity was used because it produced the strongest and most consistent results (Falgairolle et al., 2017). We have shown before that illuminating WT or *En1*-GFP preparations can affect the locomotor-like activity (Falgairolle et al., 2017; Falgairolle and O'Donovan, 2019). Therefore, experiments were also performed in preparations devoid of opsins in this study. For all animals, two to five trials were used per experiment. For locomotor-like activity induced by electrical stimulation, we used trials with and without illumination to identify the light-dependent changes. For drug-induced fictive locomotion, 3 min trials were used comprising 60 s pre-light, 60 s with the light on, and 60 s post-light. When the light was turned on or off, transient slow artifacts were produced into the extracellular recordings, and therefore were corrected manually using Clampfit (Molecular Devices) using the adjust baseline feature (Falgairolle et al.,

2017). Furthermore, the train used for the blue light produced small and short artifacts in the extracellular recordings (obscuring the raw signal). These were reduced or eliminated by generating an average shape of the artifact per file, which was subtracted from the raw data (Falgairolle et al., 2017).

Immunohistochemistry. Preparations were fixed in 4% PFA for at least 4 h at room temperature. They were then embedded in 5% agar and sectioned transversely (60 μm) on a V1000 vibratome (Leica Biosystems). The sections were then blocked in 10% normal donkey serum in 0.01 M PBS with 0.1% Triton X-100 (PBS-T) for 1.5 h and subsequently incubated overnight at room temperature in different combinations of the following antibodies: chicken anti-GFP antibody (ab13970, dilution 1:1000, Abcam), rabbit anti-RFP antibody (ab62341, dilution 1:1000), and rabbit anti-calbindin D28k antibody (dilution 1:2000, Swant). The following day, the sections were washed with PBS-T for 1 h and then incubated for 3 h with secondary antibodies: donkey anti-chicken-FITC, donkey anti-rabbit-Dylight-405 (dilution 1:100, Jackson ImmunoResearch Laboratories). The sections were then mounted on slides and coverslipped with a glycerol/PBS solution (3:7). Images were acquired using an LSM510 or LSM800 Carl Zeiss confocal microscope with 10× (air) and 40× (oil) objectives (Light Imaging Facility, National Institute of Neurological Disorders and Stroke).

Experimental design and analysis. To compare electrophysiological recordings across trials and experiments, the recordings were aligned to the beginning of the light during drug-induced locomotor-like activity, keeping 55 s before and after the light for the analysis. For stimulation, the recordings were aligned to the first stimulus, and the analysis for the dorsal root stimulation was done on 15.5 s of the recording (1.5 s before and 14 s after the first stimulus). For the brainstem stimulation, the analysis was performed on 28 s of the recording (3 s before and 25 s after the first stimulus). The signals were then analyzed using wavelets (Mor and Lev-Tov, 2007; Falgairolle et al., 2017; Falgairolle and O'Donovan, 2019). Analysis was performed on either the slow potentials, the integrated neurograms, or both. Slow potentials were obtained by band-passed filtering the raw data from 0.01 to 5 Hz. The raw data were integrated by high-pass filtering at 10 Hz, rectification, and then low-pass filtering at 5 Hz for drug-induced fictive locomotion or at 20 Hz for stimulus-evoked fictive episodes. Wavelet spectrograms (3200 points along the time dimension) were then generated. As the wavelet analysis produces artifacts (edge effects), 10 s at the beginning and the end of the spectrograms was removed for drug-induced locomotion. Locomotor-like activity evoked by dorsal root afferent stimulation does not start immediately after the first stimulus; only 7 s of the record was analyzed starting at 3 s after the first stimulus. For brainstem stimulation, 15 s of the evoked activity was analyzed starting at 5 s after the first stimulus. Time-series of frequency as well as of the phasing between the bilateral flexor–dominated ventral roots (L1/2) and between the ipsilateral flexor–dominated (L1/2) and extensor–dominated L5 ventral roots were extracted from the spectrograms. We then calculated the mean values of frequency and phasing before and during the light. The post-illumination analyses were performed only for drug-induced locomotor-like activity. The frequency time-series was then normalized by dividing by the average frequency before the light was turned on, and 1 was subtracted to set the control value to an average of 0. It was subsequently multiplied by 100 to be expressed as a percentage change. This allowed us to monitor the changes occurring on illumination and making the time-series independent of the initial frequency, allowing us to compare the effect of the light across experiments and animals. A negative value reflects the percentage decrease in the frequency, whereas a positive value reflects the percentage increase in the frequency. For drug-induced fictive locomotion, the integrated neurograms were resampled at 19 Hz to keep the same timescale as the wavelet analysis and were also expressed as a percentage change. Both the normalized frequency and integrated neurograms time-series were then averaged across trials, and then across experiments. The *n* value represents the number of experiments. To compare statistically the time-series, we used a bootstrap *t* test (Falgairolle et al., 2017). The bootstrap was iterated 10,000 times. We then plotted the two conditions that were compared, and color-coded the results with black for not statistically significant, green for $p < 0.05$, yellow for $p < 0.01$, orange for $p < 0.001$, and red for $p < 0.0001$.

We defined the beginning and the end of a burst as 40% of the distance between the trough and the peak of the integrated neurogram. Once calculated, we could then extract the duration of the bursts and the interburst intervals. We also calculated the amplitude of the burst (peak–trough). To compare the values between trials and across experiments, we averaged the variables per trial before the light, during the light, and after the light (for the drug-induced fictive locomotion only). The variables were then normalized by setting the average before the light to 0 and multiplied by 100 to be expressed as a percentage change. We also averaged all the cycle measurements across trials to get one value per experiment and then averaged the resulting values across experiments. All statistics were done using Prism 8.0 (GraphPad Software), except for the circular statistics, which were done with the MATLAB (The MathWorks) circular statistic package (https://github.com/circstat/circstat-matlab) (Berens, 2009). To compare the mean values under the different conditions (light on/off–light status; animal type–genetic identity), we used parametric statistics after verifying that the data were normally distributed (repeated-measures *t* test, *t* test, repeated-measures one-way ANOVA, one-way ANOVA, repeated-measures two-way ANOVA, or two-way ANOVA) with a two-stage linear step-up procedure of Benjamini, Krieger, and Yekutieli *post hoc* test unless specified otherwise. All results are given as mean ± standard deviation (SD).

To visualize the interneurons, we used mice in which the dorsal horn was removed (Falgairolle et al., 2017; Falgairolle and O'Donovan, 2019). The exposed cells were labeled with the calcium-sensitive dye, fura-2 AM (100 or 200 μM, Invitrogen), which was dissolved in DMSO (0.2% or 1%) together with pluronic F-127 (1% or 20%, Sigma-Aldrich) and added to the aCSF. We also added 0.1% of PowerLoad (Invitrogen) and 50 μM of MK-571, a multidrug resistance-associated protein (Antri et al., 2011). The cord was then incubated in this solution for at least half an hour before being transferred to the recording chamber with regular aCSF. Locomotor-like activity was evoked with NMDA (5 μM), 5-HT (10 μM), and DA (50 μM) and monitored with extracellular recordings of the ventral roots. Fluorescence images were obtained using a QuantEM 512SC (Photometrics) and illuminated using a Xenon lamp and a UV filter (excitation: 380, emission: 490-530). As fura-2 AM is a ratiometric dye, it has 2 peaks of excitation. The wavelength we used for exciting fura-2 AM (380 nm) produces a stronger fluorescent signal when the dye is not bound to calcium and which declines on calcium binding. At least two trials of 90 s were recorded (4 Hz) per location on the dorsal cut surface.

The analysis was performed with MATLAB and the plugin MIJI (Fiji for MATLAB) (Schindelin et al., 2012). As the calcium signals were opposite to traditional recordings (decreased fluorescence on calcium binding), we inverted the signal. Then, the movie frames were registered to decrease movement artifacts during the acquisition. We used a descriptor-based series registration (Preibisch et al., 2010) with translation as a transformation model, and the registration was done against the first frame only. We then corrected for bleaching and calculated the mean, maximum, minimum, and SD projected images. We subsequently removed the minimum projected image from the bleach-corrected movie and again calculated the mean, maximum, and minimum projected image. Each of the projected images was binarized; only areas with >40 pixels were kept. Finally, all the binary images were merged to create the binary image used for the analysis. Therefore, all cells or areas that had calcium dye in them were detected independently of being active or not. ROIs were then extracted from the binary image, and therefore were not always representative of a neuron. All calculations were subsequently done on the registered movie before any corrections. For each ROI, an average pixel value was calculated for each frame, therefore creating a time-series per ROI (f). Each time-series was corrected for bleaching by fitting a mono-exponential function to the data and subtracting it. We then calculated the minimum of each time-series (f_0) and calculated $\Delta f = \frac{f - f_0}{f_0} * 100$ for each ROI. We then filtered the data and discarded ROIs based on the following procedures. First, we calculated the frequency and the power density of each signal (Δf). Signals that exhibited a frequency much slower or higher than the locomotor

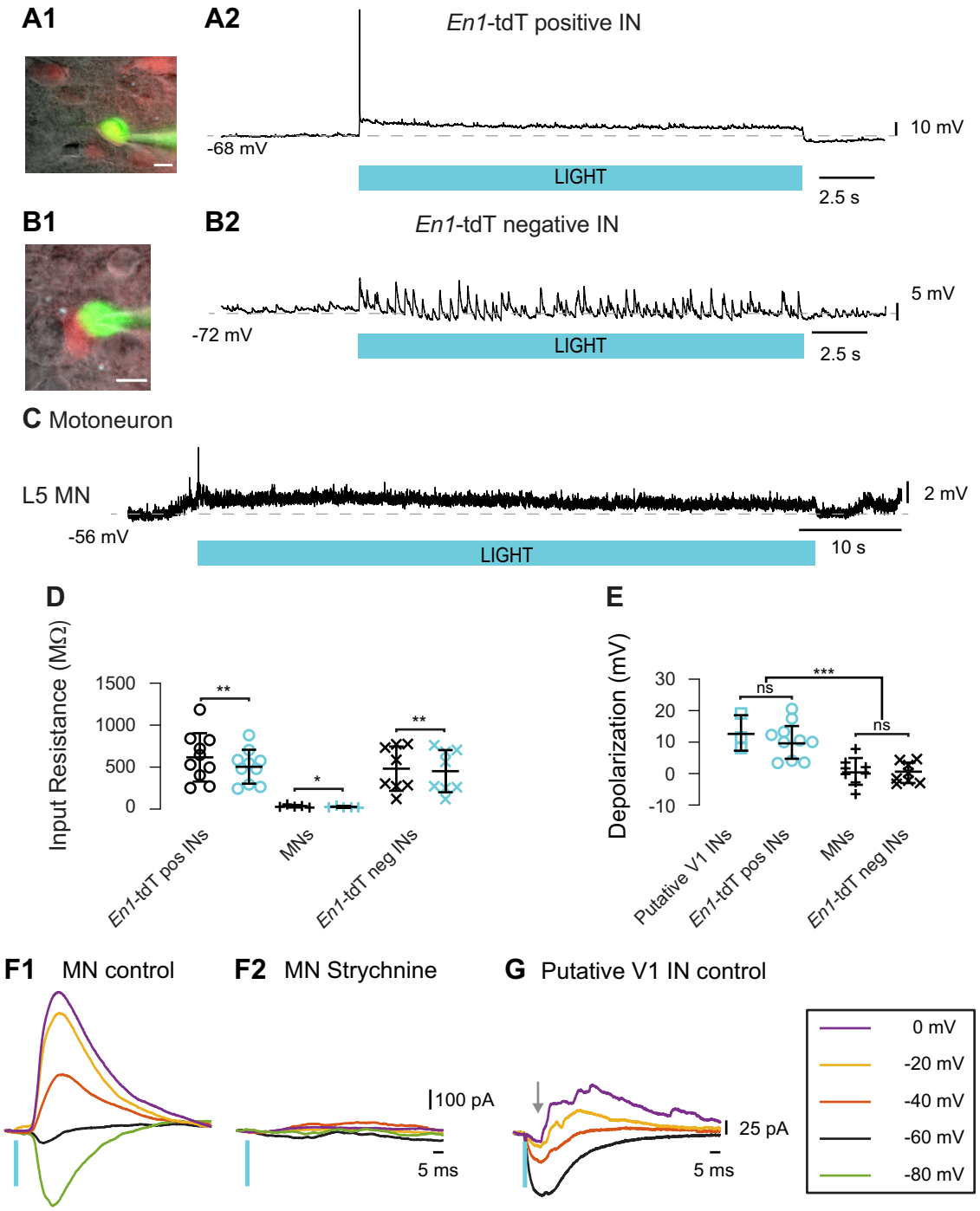

Figure 1. Intracellular recordings of V1-positive and -negative interneurons and MNs in *En1*-ChR2-EYFP-tdt and *En1*-ChR2-EYFP cords during light-induced depolarization of V1s. ***A1***, High-contrast, bright-field image on which a tdT fluorescence image and a green fluorescence image are superimposed showing the electrode and an *En1*-tdT-positive (pos) interneuron (IN) filled in green in an *En1*-ChR2-EYFP-tdt dorsally shaved spinal cord. White scale bar, 6 μm. ***A2***, Whole-cell recording of the interneuron shown in ***A1***, showing depolarization during illumination. Blue bar below the recording represents the duration of the light. ***B1***, High-contrast, bright-field image on which a tdT fluorescence image and a green fluorescence image are superimposed, showing the electrode and an *En1*-tdT-negative interneuron filled in green from an *En1*-ChR2-EYFP-tdt dorsally shaved spinal cord. White scale bar, 6 μm. ***B2***, Whole-cell recording of the interneuron shown in ***B1***, showing a barrage of evoked synaptic potentials superimposed on a slow hyperpolarization during illumination. Blue bar below the recording represents the duration of the light. ***C***, Whole-cell recording of a MN showing a small depolarization during illumination. Blue bar below the recording represents the duration of the light. ***D***, Input resistance of all the neurons recorded intracellularly for this study under control conditions (black) or during light illumination (blue). They have been separated according to their putative identity. Input resistances were compared in control conditions versus illumination: paired *t* test: *En1*-tdT-positive interneurons (pos INs; $n = 10$ neurons in 3 preparations): $p = 0.0077$, MNs ($n = 5$, in 2 preparations): $p = 0.0388$, *En1*-tdT-negative interneurons (neg INs; $n = 8$ neurons in 3 preparations): $p = 0.0062$. ***E***, Plot represents the light-induced depolarization for all neurons recorded in this study. Putative V1s and *En1*-tdT-positive interneurons showed the strongest depolarization to the light, whereas MNs and *En1*-tdT-negative interneurons showed variable responses: one-way ANOVA, $F_{(3,25)} = 12.44$, $p < 0.0001$, multiple comparisons: *En1*-tdT-positive interneurons (10 neurons in 3 preparations) versus putative V1 interneurons (3 neurons in 2 preparations) $p = 0.3222$, *En1*-tdT-positive versus MNs (8 in 4 preparations) $p = 0.0002$, *En1*-tdT-positive versus *En1*-tdT-negative (8 neurons in 3 preparations) $p = 0.0001$, putative V1 interneurons versus MNs $p = 0.0005$, putative V1 interneurons versus *En1*-tdT-negative interneurons $p = 0.0003$, MNs versus *En1*-tdT-negative interneurons $p = 0.8406$. ***F1***, Voltage-clamp recording of a MN in an *En1*-ChR2 spinal cord using intracellular QX-314 to block action potentials. Depolarization of V1 interneurons for 1 ms (blue bar represents the duration of the light) induced synaptic potentials in the MN. ***F2***, Voltage-clamp recording of the same MN in the presence of 5 μM of strychnine, a glycinergic antagonist. ***G***, Voltage-clamp recording of a putative V1 interneuron in an

frequency were discarded. We then selected signals that showed only strong power density at a frequency slower than 1.2 Hz. The remaining signals were sorted to keep only those that were coherent with the rhythmic activity recorded from the ventral roots (Kwan et al., 2010). With those, we calculated the phasing of each optical signal with reference to one of the extracellular ventral root recordings (typically left L5). Finally, the signals were separated in six groups according to their phases ($330° \leq$ phase $< 30°$, $30° \leq$ phase $< 90°$, $90° \leq$ phase $< 150°$, $150° \leq$ phase $< 210°$, $210° \leq$ phase $< 270°$, $270° \leq$ phase $< 330°$).

Results

To establish that the expression of ChR2 in *En1* interneurons was specific, we generated mice that coexpressed ChR2 (EYFP, membrane-bound) and tdTomato (tdT, cytoplasmic). We found that ChR2 was expressed densely in processes in the ventral part of the cord in both the L2 and L5 segments ($n = 3$) and was colocalized with tdT (data not shown). We also confirmed that ventrally located calbindin-positive neurons (putative Renshaw cells) coexpress ChR2 and tdT consistent with earlier work with this mouse line (Gosgnach et al., 2006; Britz et al., 2015; Falgairolle and O'Donovan, 2019). Collectively, these results indicate that ChR2 is expressed specifically in *En1*-cre-positive neurons.

Intracellularly recorded responses in MNs, other V1 interneurons, and non-V1 interneurons induced by activation of ChR2 in V1 interneurons

ChR2 is a light-sensitive sodium channel that depolarizes the cells in which it is expressed on illumination. Therefore, we next performed experiments to verify that V1 interneurons (tdT-positive) are depolarized when excited by a blue light. To gain access to V1s, we ablated the dorsal horn of the lumbar cord as described previously (Falgairolle and O'Donovan, 2019). Ten tdT-positive interneurons were targeted that exhibited an average depolarization of 9.92 ± 5.2 mV (ranging from 3.34 to 19.07 mV; *En1*-tdT-positive INs; Fig. 1*A*,*E*) on exposure to light, whereas the average of 8 tdT-negative interneurons exposed to light was 0.24 ± 3.24 mV (ranging from −3.24 to 4.6 mV; *En1*-tdT-negative INs; Fig. 1*B*,*E*).

In addition, neurons were targeted blindly in whole *En1*-ChR2 cords. In response to light, 8 MNs (identified by an antidromic spike) showed an average response of 0.70 ± 4.26 mV (ranging from −6.53 to 7.81 mV; Fig. 1*E*), whereas 3 putative V1 interneurons exhibited an average depolarization of 12.91 ± 5.2 mV (ranging from 8.1 to 19.12 mV; Fig. 1*E*). We also found that interneurons and MNs received inputs from V1s that lasted for the duration of the illumination and were accompanied by a decreased input resistance (Fig. 1*B*,*C*). Surprisingly, although V1s have been shown to be inhibitory, some MNs and interneurons showed small depolarizing responses on illumination (3.77 ± 2.8 mV from 4 of 8 recorded MNs and 3.88 ± 1 mV from 3 of 8 recorded interneurons). To assess whether these responses were inhibitory, we targeted blindly neurons in *En1*-ChR2 spinal cords and recorded currents evoked by depolarizing V1 interneurons. At −60 mV, all recorded neurons (6 MNs, 4 putative V1 interneurons) showed an inward current that reversed on depolarization (Fig. 1*F1*). At −60 mV, the maximum synaptic currents were as follows: MNs, -71.83 ± 66.51 pA (range: −204 to −22.90 pA); putative V1s, -86.50 ± 45.26 (range: −138 to −41 pA). In 2 MNs, after bath application of 5 μM strychnine (a glycine receptor antagonist), all synaptic inputs resulting from V1 activation were abolished (Fig. 1*F2*). To further confirm that depolarizing V1 interneurons produced functional inhibition, we performed experiments in which all fast, inhibitory neurotransmission was blocked by using 5 μM strychnine and 20 μM bicuculline (a $GABA_A$ receptor antagonist). We found that light activation of V1s did not trigger any excitatory responses or alter the frequency of spontaneous bursting in these preparations, confirming that the vast majority of V1 interneurons in the lumbar spinal cord are inhibitory.

Light-induced depolarization of V1 interneurons decreases the frequency of drug-induced locomotor-like activity

Previous work had shown that optogenetic depolarization of V1s could silence ventral root discharge obtained during drug-induced fictive locomotion (Britz et al., 2015). This could be because of direct inhibition of MNs, inhibition of premotor excitatory interneurons, or blockade of the CPG. To address these questions, we analyzed the frequency and phasing of the locomotor activity recorded intracellularly from MNs and from slow ventral root potentials during drug-induced fictive locomotion (5 μM NMDA, 10 μM 5-HT, and 50 μM DA) (Falgairolle and O'Donovan, 2019). We first verified that phasing and frequency were not statistically different for the integrated neurograms and the slow potentials in control *En1*-GFP cords. In *En1*-ChR2 spinal cords, depolarizing V1s significantly slowed the frequency (from 0.36 ± 0.1 Hz to 0.28 ± 0.08 Hz; a decrease of $21.4 \pm 19\%$; $n = 12$) compared with *En1*-GFP cords (from 0.37 ± 0.05 Hz to 0.38 ± 0.05 Hz; a small increase of $3.9 \pm 2\%$, $n = 10$). After the light was turned off, *En1*-ChR2 preparations exhibited a transient increase in frequency and enhanced bursting (Fig. 2*A*–*C*). As previously shown (Falgairolle and O'Donovan, 2019), the duty cycle in most of these preparations was extensor-biased (larger in the extensor-dominated ventral roots than in the flexor-dominated ones). However, in 2 preparations of 12 *En1*-Chr2 spinal cords, the rhythm was flexor-biased and depolarization of V1 interneurons led to an increase in frequency. All cords, whether extensor- or flexor-biased, were extensor-biased during illumination. Because there were no statistically significant differences between the measured experimental variables (frequency, phase, burst duration, and interburst interval) between initially flexor- and extensor-biased fictive locomotion, we did not separate the two datasets for analysis. We found that V1 depolarization led to a decrease in the number of bursts, particularly at the beginning of the light (Fig. 2*A*). When rhythmic bursting could be detected during the light, it was accompanied by an increase of $22.12 \pm 32\%$ in the L5 burst duration (from 1.79 ± 0.9 s to 2.26 ± 1.4 s; $n = 12$) and a decrease of $3.1 \pm 18\%$ in the L1 burst duration (from 1.64 ± 0.6 s to 1.54 ± 0.5 s, repeated-measures one-way ANOVA, $p = 0.0282$, L1 vs L5 $p = 0.003$) compared with *En1*-GFP cords (L1: $-3.84 \pm 2.2\%$, L5: $-8.68 \pm 5.6\%$), although only the change in the L5 burst duration was significant ($p = 0.0067$). The interburst durations also increased in both L1 (from 1.45 ± 0.6 s to 2.52 ± 1.9 s, increase of $65.76 \pm 70.8\%$) and L5 (from 1.35 ± 0.5 s to 2.12 ± 1.4 s increase of $51.97 \pm 56.1\%$), which was only statistically different from the *En1*-GFP preparations in L5 ($p = 0.064$ and $p = 0.0114$, respectively). As expected, depolarizing V1 interneurons

←

En1-ChR2 spinal cord using QX-314 to block action potentials. Depolarization of V1s for 1 ms (blue bar represents the duration of the light) induced an initial inward photocurrent (gray arrow) as well as synaptic potentials in the interneuron. The different membrane potentials at which the neurons were held are color-coded is indicated in the box. $*p < 0.05$. $**p < 0.01$. $***p < 0.001$.

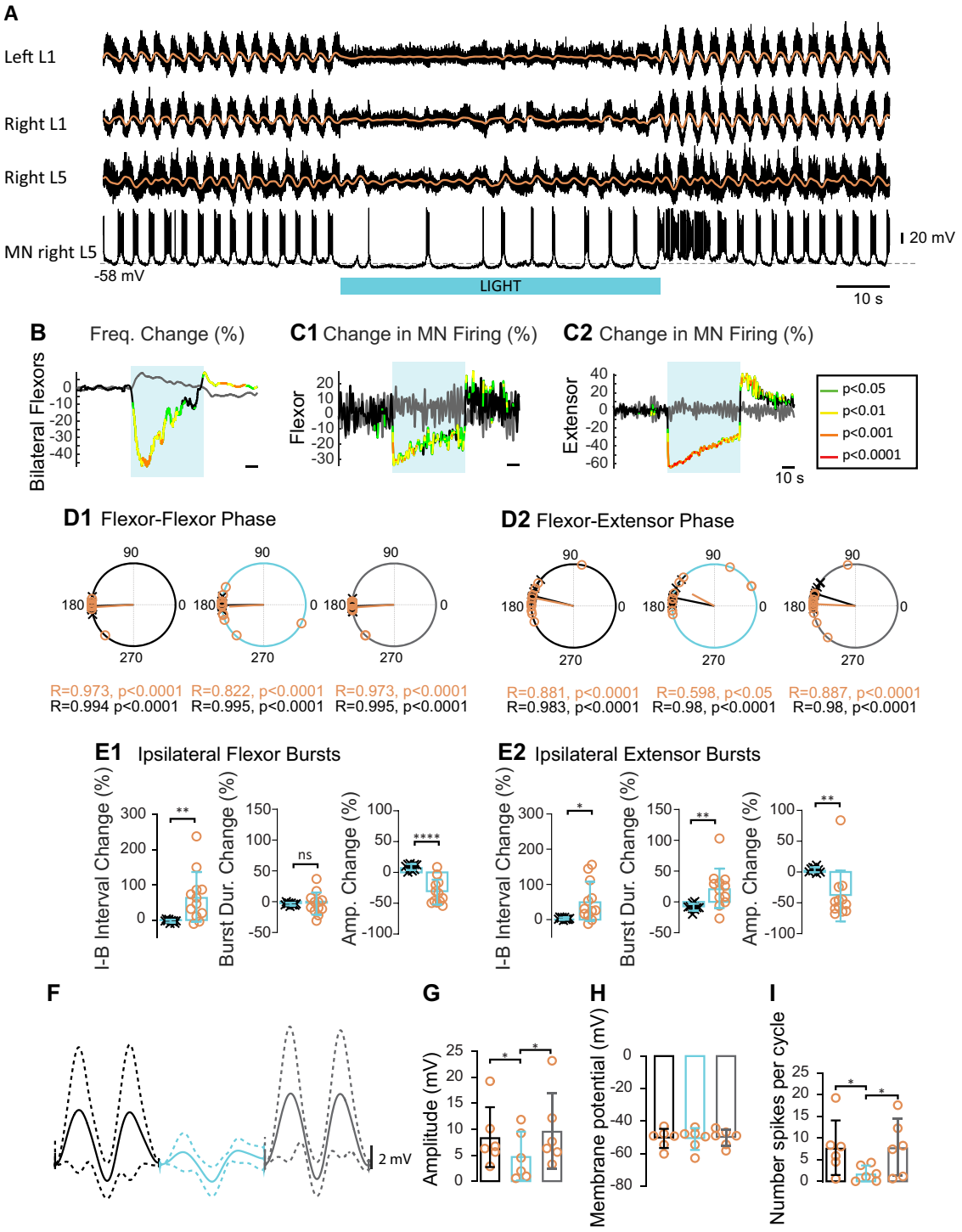

Figure 2. Light-induced depolarization of V1 neurons disrupts and decreases the frequency of drug-induced locomotor-like activity. ***A***, Locomotor-like activity recorded from the right L1 and the left L1 and L5 ventral roots (black traces) together with an intracellular recording of a flexor MN from a P2 *En1*-ChR2 isolated spinal cord. Superimposed orange traces represent the slow potentials obtained by low pass filtering the raw signals. Locomotor-like activity was induced by bath-applying 5 μM NMDA, 10 μM 5-HT, and 50 μM DA. Blue bar represents the light duration (60 s). ***B***, ***C***, Time-series showing the change (%) in frequency (***B***) and averaged integrated ventral root discharge (MN firing) for the ipsilateral L1 (***C1***) and L5 ventral roots (***C2***) for the *En1*-ChR2 spinal cords (black trace) and the *En1*-GFP preparations (gray trace). The statistics were obtained using a bootstrap *t* test between *En1*-ChR2 ($n = 12$) and the *En1*-GFP ($n = 10$) cords and are color-coded as indicated in the box to the side of the records. Blue rectangle represents timing of the illumination. ***D***, Circular plots represent the phasing of the bilateral flexor (***D1***) and ipsilateral flexor-extensor (***D2***) ventral roots during fictive locomotion before (black circles), during (blue circles), and after (gray circles) illumination of *En1*-ChR2 (orange circles) and *En1*-GFP (black crosses) spinal cords. *R* is the length of the vector, and *p* is the value for the Raleigh test of uniformity. Using the Harrison–Kaji test, we calculated the statistical difference between the two types of cord (genetic identity) and the difference before, during, and after illumination (light status) for the phasing in bilateral flexor and ipsilateral flexor-extensor ventral roots. The result of the tests for the bilateral flexors were as follows: light status, $F_{(2,60)} = 0.56$, $p = 0.5764$; genetic identity, $F_{(1,60)} = 0.6$, $p = 0.4428$; interaction, $F_{(2,60)} = 0.79$, $p = 0.4575$. For the flexor-extensor phases, the results were as follows: light status, $F_{(2,60)} = 0.79$, $p = 0.4574$; genetic identity, $F_{(1,60)} = 1.69$, $p = 0.1983$; interaction, $F_{(2,60)} = 1.2$, $p = 0.3083$. ***E1***, Light-dependent changes in flexor ventral root bursts, ipsilateral to the recorded extensor ventral root for *En1*-ChR2 (orange circles, $n = 12$) and *En1*-GFP (black crosses, $n = 10$) cords. Bar plots represent the changes (%) of the interburst (I-B) interval (left), burst duration (middle), and amplitude (right) during illumination (blue rectangle) compared with before the light. ***E2***, Similar measurements as for ***E1*** for the L5 ventral roots ipsilateral to the recorded L1 ventral roots. Repeated-measures two-way ANOVA was used to statistically compare the interburst interval, burst duration (burst

decreased significantly MN firing with the biggest decrease in the L5 segment (~30% in L1 vs ~60% in L5, $n = 12$; Fig. 2*C*) compared with the *En1*-GFP preparations. However, the burst amplitude (from trough to peak) decreased in a similar manner in L1 and L5 (by 31.92 ± 20.2% and by 38.77 ± 41.3%, respectively, two-way ANOVA, $p = 0.6124$).

Depolarizing V1 interneurons disrupted the activity in all the recorded roots; but when the phase could be measured from the slow potentials, it was maintained in the bilateral L1 roots compared with the *En1*-GFP preparations (control: 183.6 ± 13, light: 183.17 ± 34, after light: 183.9 ± 13) but was slightly altered in the L1-L5 roots (control: 168.4 ± 28, light: 151.66 ± 51, after light: 177.33 ± 27; Fig. 2*D*). The membrane potential of individual MNs (5 extensor and 1 flexor) recorded from the L5 segment did not change significantly when V1 neurons were depolarized by light (control: −50.68 ± 5.9 mV, light: −51.04 ± 6.8 mV, after light: −50.28 ± 5.1 mV; Fig. 2*H*). In these MNs, the locomotor drive potentials were reduced during illumination (from 8.47 ± 5.76 mV to 4.84 ± 4.69 mV; Fig. 2*F*,*G*) and recovered after the light was turned off. Consequently, their firing was also reduced during illumination (from 7.76 ± 6.3 to 1.82 ± 1.84 spikes/cycle; Fig. 2*I*).

Because there were so few bursts during the light, it was possible that the light was disrupting the function of the generator rather than modulating its frequency. Therefore, to establish whether depolarization of V1 neurons did indeed regulate frequency, we varied the intensity of the light and measured the effects on the locomotor frequency ($n = 5$). We found that there was a proportional change in the frequency of the rhythm according to the light intensity, and that even at 10% of the maximum intensity, depolarizing V1s led to a decrease, albeit small, in the frequency of the rhythm.

Another complication of these experiments is that the *En1* transcription factor is expressed throughout the CNS and could be present in the synaptic terminals of descending or propriospinal axons. To address this issue, we performed the same experiments as described above but directed the illumination onto the thoracic segments to depolarize descending or propriospinal *En1*$^+$ axons ($n = 4$ cords). Under these conditions, the rhythm was not disturbed, but we measured a small decrease in the frequency of the rhythm during the light (5.25 ± 6.1%) that was smaller than that observed when illuminating the lumbar cord (*t* test with Welch correction, $p = 0.0208$). It is not clear whether this decrease in frequency is because of the effect of the light on *En1*$^+$ axons in the thoracic segments or because some of the light was diffracted onto the upper lumbar segments. Nevertheless, these results strongly suggest that the effects of light on the lumbar cord were because of actions on local V1s.

Activation of V1 interneurons in hemicords decreases the frequency of the rhythm

Because it lacks contralateral inputs, the hemicord offers a unique opportunity to simplify the rhythmogenic circuitry and to clarify the role of V1 interneurons in locomotor function. In a previous paper, we showed that V1s are active in hemicords and that hyperpolarizing them optogenetically accelerates the locomotor rhythm compared with the slowing seen in whole-cord preparations (Falgairolle and O'Donovan, 2019). Therefore, we hypothesized that depolarizing V1 interneurons would produce the opposite effects of hyperpolarization in the hemicords.

During rhythmic activity induced with 5 μM NMDA, 10 μM 5-HT, and 50 μM DA, we found that depolarizing V1 interneurons significantly decreased the frequency of the rhythm (~20%; Fig. 3*A*,*B*; $n = 8$) compared with the results obtained in WT hemicords (data not shown). There was an increase of the interburst interval of the L1 ventral root (119.8 ± 39.1%, from 3.4 ± 0.9 s to 7.21 ± 0.9 s), which was accompanied by an increase in the burst duration of the L5 ventral root (126 ± 54.1%, from 3.28 ± 0.8 s to 7.1 ± 0.9 s). By contrast, there was no significant change in the interburst interval of the L5 root (−2.3 ± 22.5%, from 3.21 ± 0.8 s to 3.12 ± 0.9 s) or the duration of the L1 ventral root (1.27 ± 24.3%, from 3.14 ± 0.6 s to 3.1 ± 0.6 s compared with WT; Fig. 3*F*,*G*). The asymmetrical changes between the L1 and L5 ventral roots in the *En1*-ChR2 spinal cords were significantly different (two-way ANOVA $p < 0.0001$ for both). In these experiments, the duty cycle during illumination became extensor-biased ($n = 8$; Fig. 3*E*). Compared with the effect of light on the *En1*-ChR2 whole cords, the rhythm was less disturbed, with MN firing being decreased most prominently in L5 ventral roots (Fig. 3*C*). Furthermore, the amplitude of the bursting was increased in the L1 ventral root (13.28 ± 9.5%) and decreased in the L5 ventral root (−40.83 ± 9.98%, $p < 0.0001$). There was also a statistically significant change in the ipsilateral flexor and extensor phasing when the light was turned on (Fig. 3*D*; Watson–Williams test, $p = 0.0143$). Because we measured the phasing on the bursting, we were concerned that the change in phasing could be due in part to the asymmetrical effect of the light on the amplitude of the flexor and extensor bursts. The light increased the amplitude of the L1 flexor-dominated bursts and decreased the amplitude of the L5 extensor-dominated bursts. If the same phenomenon occurred in the flexor MNs present in the L5 ventral root, it would appear as a burst in phase with the L1 root without a phase change of the extensor MN activity. When we performed the phase analysis on the slow potentials, no phase change was observed and, therefore, the change in phasing measured from the bursting is probably not physiological.

We also tested whether the effect of the light on the cords depended on the initial frequency of the rhythm. To do this, we plotted the initial control frequency (pre-light) against the frequency during the light for WT and *En1*-ChR2 hemicords, as well as *En1*-GFP and *En1*-ChR2 whole cords (Fig. 3*H*). We found that the light itself had little or no effect on the frequency of the rhythm in control (*En1*-GFP) and WT hemicords because all the data points lay on the line of unity. By contrast, depolarization of V1 interneurons decreased the frequency in the *En1*-ChR2 whole cords proportional to the initial frequency, so that

←

dur.), and burst amplitude (Amp) change between L1 and L5 ventral roots in *En1*-ChR2 and *En1*-GFP preparations before, during, and after illumination. Interburst interval (light status, $F_{(1.009,40.37)} = 16.36$, $p = 0.0002$; root and genetic identity, $F_{(3,40)} = 4.862$, $p = 0.0056$; all data, $F_{(40,80)} = 1.025$, $p = 0.4521$; interaction, $F_{(6,80)} = 6.264$, $p < 0.0001$); burst duration (light status, $F_{(1.092,43.66)} = 0.2664$, $p = 0.629$; root and genetic identity, $F_{(3,40)} = 3.818$, $p = 0.017$; all data, $F_{(40,80)} = 0.882$, $p = 0.6638$; interaction, $F_{(6,80)} = 6.834$, $p < 0.0001$); and burst amplitude (light status, $F_{(1.171,46.85)} = 29.15$, $p < 0.0001$; root and genetic identity, $F_{(3,40)} = 4.351$, $p = 0.0096$; all data, $F_{(40,80)} = 1.031$, $p = 0.4434$; interaction, ($F_{(6,80)} = 14.32$, $p < 0.0001$). ***F***, Cycle-triggered average (continuous line, 2 cycles) and SD (dotted lines) of the synaptic drive to a MN during fictive locomotion in *En1*-ChR2 spinal cords before (black), during (blue), and after (gray) illumination. ***G***, Bar plot represents the amplitude of the synaptic drive before (black rectangle), during (blue rectangle), and after (gray rectangle) the light (repeated-measures one-way ANOVA: light status, $F_{(1.155,5.776)} = 10.05$, $p = 0.0186$; spinal cords, $F_{(5,10)} = 26.32$, $p < 0.0001$). ***H***, Bar plot represents the membrane potential as in ***G*** (repeated-measures one-way ANOVA: light status, $F_{(1.165,5.827)} = 0.7734$, $p = 0.4345$; spinal cords, $F_{(5,10)} = 91.82$, $p < 0.0001$). ***I***, Bar plot represents the number of spikes per cycle as in ***G*** (repeated-measures one-way ANOVA: light status, $F_{(1.337,6.686)} = 6.241$, $p = 0.0369$; spinal cords, $F_{(5,10)} = 5.410$, $p = 0.0115$). *$p < 0.05$. **$p < 0.01$. ****$p < 0.0001$.

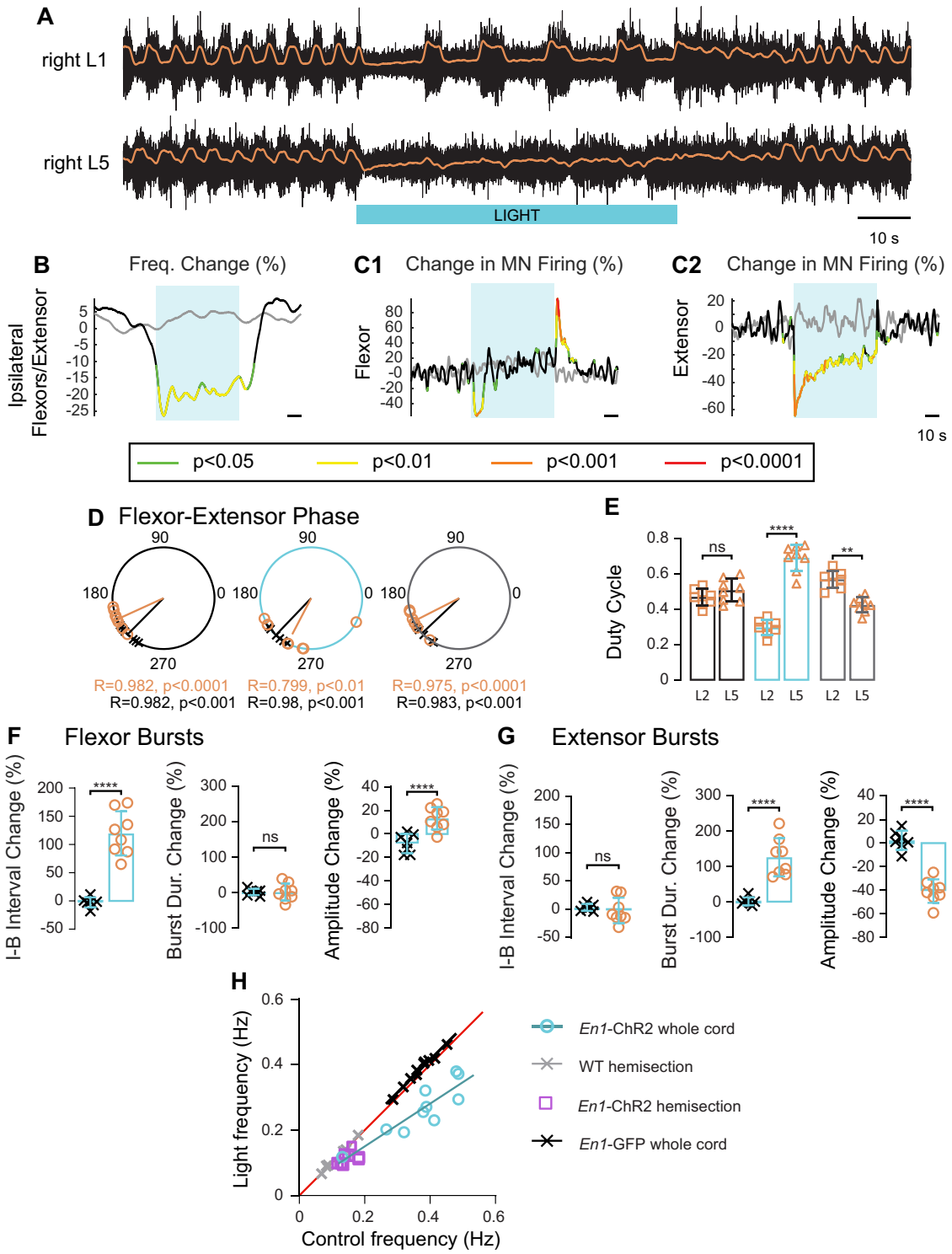

Figure 3. Light-induced depolarization of V1 interneurons decreases the frequency of drug-induced locomotor-like activity in *En1*-ChR2 hemicords. ***A***, Motor activity recorded from the right L1 and L5 ventral roots in a hemisected spinal cord from an *En1*-ChR2 mouse. Black traces represent the high pass (10 Hz) filtered neurograms. Superimposed orange traces represent the integrated neurograms. Rhythmic motor activity was induced by applying 5 μM NMDA, 10 μM 5-HT, and 50 μM DA. Blue bar below the records represents the light duration (60 s). ***B***, ***C***, Time-series showing the change (%) in frequency (***B***) and the averaged integrated ventral root discharge (MN firing) for the ipsilateral L1 (***C1***) and L5 ventral roots (***C2***) for the *En1*-ChR2 spinal cords (black traces) and the WT preparations (gray traces). The statistics were obtained using a bootstrap *t* test between *En1*-ChR2 ($n = 8$) and the WT ($n = 7$) cords and are color-coded as indicated in the box below the records. Blue rectangle represents the timing of illumination. ***D***, Circular plots represent the phasing of the ipsilateral flexor-extensor ventral roots during motor activity before (black circles), during (blue circles), and after (gray circles) illumination of *En1*-ChR2 (orange circles) and WT (black crosses) spinal cords. *R* is the length of the vector, and *p* is the value for the Raleigh test of uniformity. Using the Harrison–Kaji test, we calculated the statistical difference between the two types of cord (genetic identity) and the difference before, during, and after illumination (light status) for the phasing in bilateral flexor and ipsilateral flexor-extensor ventral roots. The result of the test for the flexor-extensor phases was as follows: light status, $F_{(2,39)} = 3.65$, $p = 0.0351$; genetic identity, $F_{(1,39)} = 1.43$, $p = 0.2385$; interaction, $F_{(2,39)} = 4.66$, $p = 0.0154$. We then performed a Watson–Williams test to compare the *En1*-ChR2 flexor-extensor phasing before, during, and after the light ($F_{(2,21)} = 5.24$, $p = 0.0143$) and performed the same test for the WT ($F_{(2,18)} = 0.11$, $p = 0.982$). We also compared the *En1*-ChR2 and the WT before, during, and after illumination using the Watson–Williams test ($F_{(1,13)} = 11.84$, $p = 0.0044$; $F_{(1,13)} = 1.06$, $p = 0.3216$; $F_{(1,13)} = 6.25$, $p = 0.0266$; respectively). ***E***, Duty cycle of the flexor

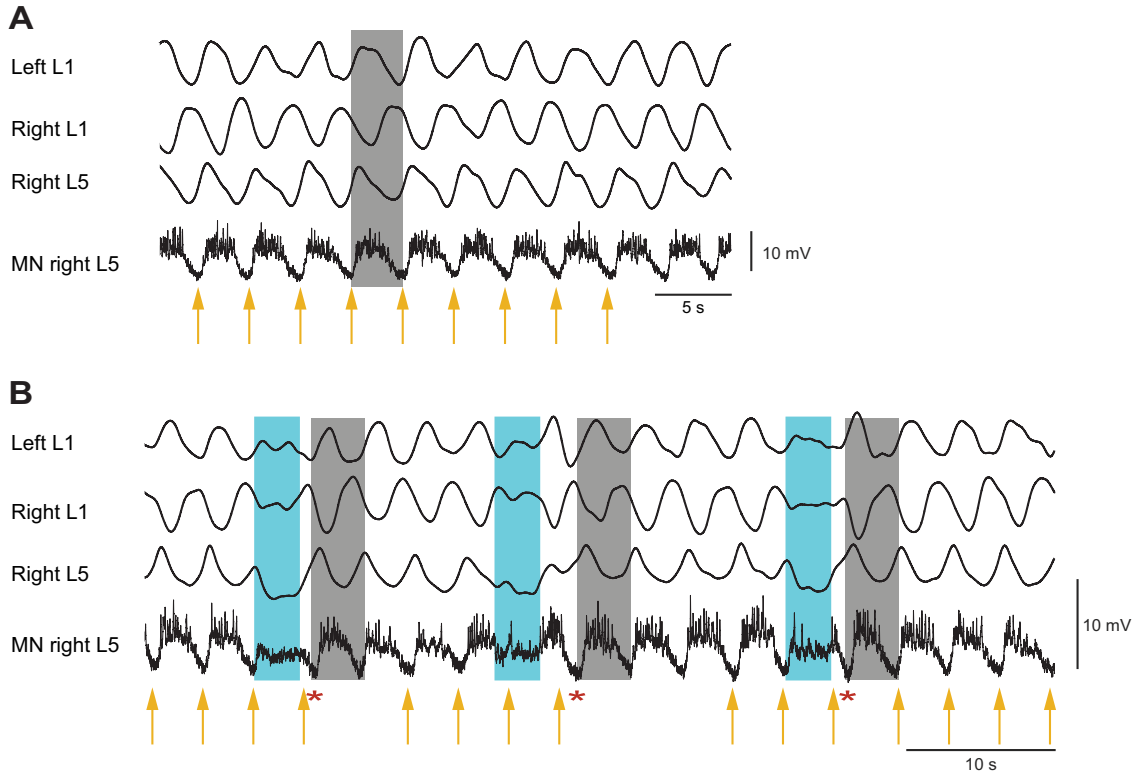

Figure 4. Transiently depolarizing V1 interneurons reset the drug-induced locomotor-like rhythm. ***A***, Integrated neurograms extracted from locomotor-like activity recorded from the right and left L1 and the L5 ventral roots (black traces) together with an intracellular recording of an extensor MN (action potentials were digitally removed) from an *En1*-ChR2 spinal cord. Locomotor-like activity was induced by applying 5 μM NMDA, 10 μM 5-HT, and 50 μM DA. Yellow arrows identify the trough of the synaptic drive. The arrows are evenly spaced. ***B***, The same recording as in ***A***, but with transient illumination of the lumbar spinal cord (blue rectangles). Yellow arrows have the same spacing as in ***A***. Red asterisks indicate when the arrows do not point to a trough because the onset of the next burst in both the MN and the ventral roots is delayed. Gray rectangles emphasize that, after the light is turned off, the rhythm is locomotor-like with bilateral L1 and L1/L5 bursts alternating.

←

(L2, orange squares) and the extensor (L5, orange triangles) cycles in *En1*-ChR2 spinal cords before (black rectangles), during (blue rectangles), and after (gray rectangles) illumination (repeated-measures two-way ANOVA: light status, $F_{(1.538,21.53)} = 0.1884$, $p = 0.7725$; root identity, $F_{(1,14)} = 17.37$, $p = 0.0009$; all data, $F_{(14,28)} = 4.379$, $p = 0.0004$; interaction, $F_{(2,28)} = 209.7$, $p < 0.0001$). ***F***, Light-dependent changes in flexor ventral root bursts for *En1*-ChR2 (orange circles) and WT (black crosses) cords. Bar plots represent the changes (%) of the interburst (I-B) interval (left), burst duration (Dur; middle), and amplitude (Amp; right) during illumination (blue rectangle) compared with before the light. ***G***, Similar measurements as for ***F*** for the extensor ventral roots. Repeated-measures two-way ANOVA was used to statistically compare the interburst interval, burst duration, and burst amplitude change between flexor and extensor ventral roots in *En1*-ChR2 and WT preparations before, during, and after illumination. I-B interval (light status, $F_{(1.453,37.77)} = 39.18$, $p < 0.0001$; root and genetic identity, $F_{(3,26)} = 18.88$, $p < 0.0001$; spinal cords all data, $F_{(26,52)} = 1.621$, $p = 0.069$; interaction, $F_{(6,52)} = 61.56$, $p < 0.0001$); burst duration (light status, $F_{(2,52)} = 26.37$, $p < 0.0001$; root and genetic identity, $F_{(3,26)} = 15.70$, $p < 0.0001$; spinal cords all data, $F_{(26,52)} = 1.322$, $p = 0.1933$; interaction, $F_{(6,52)} = 36.82$, $p < 0.0001$); and amplitude (light status, $F_{(1.511,39.19)} = 9.663$, $p = 0.0011$; root and genetic identity, $F_{(3,26)} = 25.48$, $p < 0.0001$; all data, $F_{(26,52)} = 0.8785$, $p = 0.6324$; interaction, $F_{(6,52)} = 31.28$, $p < 0.0001$). ***H***, Plot represents the frequency of the rhythm before the light (control frequency) plotted against the frequency of the rhythm during the light (light frequency) in *En1*-ChR2 whole cords (blue circles), *En1*-ChR2 hemicords (purple squares), *En1*-GFP (black crosses), and WT hemisected (gray crosses) cords. Red line indicates the line of unity where the frequency is the same before and during light. Lines indicate the linear regressions calculated for the experiments. *En1*-GFP whole cords ($n = 10$; Pearson correlation $r = 0.9861$, $p < 0.0001$, slope: 1.002x + 0.01438); WT hemicords ($n = 7$; Pearson correlation $r = 0.9958$, $p < 0.0001$, slope: 0.9906x − 0.003275); *En1*-ChR2 whole cords ($n = 10$; Pearson correlation $r = 0.8885$, $p = 0.0006$, slope: 0.6528x + 0.01985); and *En1*-ChR2 hemicords ($n = 8$; Pearson correlation $r = 0.4513$, $p = 0.0029$). $^{**}p < 0.01$. $^{****}p < 0.0001$.

the largest decreases occurred at the highest frequencies. In *En1*-ChR2 hemicords, there was no relationship between the initial frequency and the change in frequency.

V1 interneurons target the CPG

The previous results, showing that manipulation of V1s can modulate the locomotor frequency, suggest that V1 neurons target the CPG. To test this idea, we use a short optical stimulus (duration between 1 and 2 s) to establish whether a brief depolarization of V1 neurons would reset the rhythm (Winfree, 1975; Duysens, 1977; Ayers and Selverston, 1979; McClellan and Jang, 1993).

We found that depolarization of V1 interneurons during ongoing locomotor-like activity led to a delay in the appearance of the next burst (Fig. 4; $n = 5$ intracellular MNs, and $n = 9$ ventral root neurograms) and therefore the next locomotor cycle, consistent with V1s targeting the CPG.

Previous work had shown that light could silence rhythmic ventral root activity in cords in which V1s expressed channelrhodopsin, and this was attributed to direct inhibition of MNs by $En1^{+}$ Renshaw cells (Britz et al., 2015). However, if V1 interneurons modulate the frequency of the CPG, then all interneurons (including those of the CPG) that exhibit locomotor-like behavior should be affected during V1 depolarization. This would mean that the silencing of MNs observed by Britz et al. (2015) was because of inhibition of the rhythm generator rather than MNs. To test this idea, we performed calcium imaging experiments on interneurons loaded with the calcium-sensitive dye fura-2 AM. For this purpose, we removed the dorsal part of

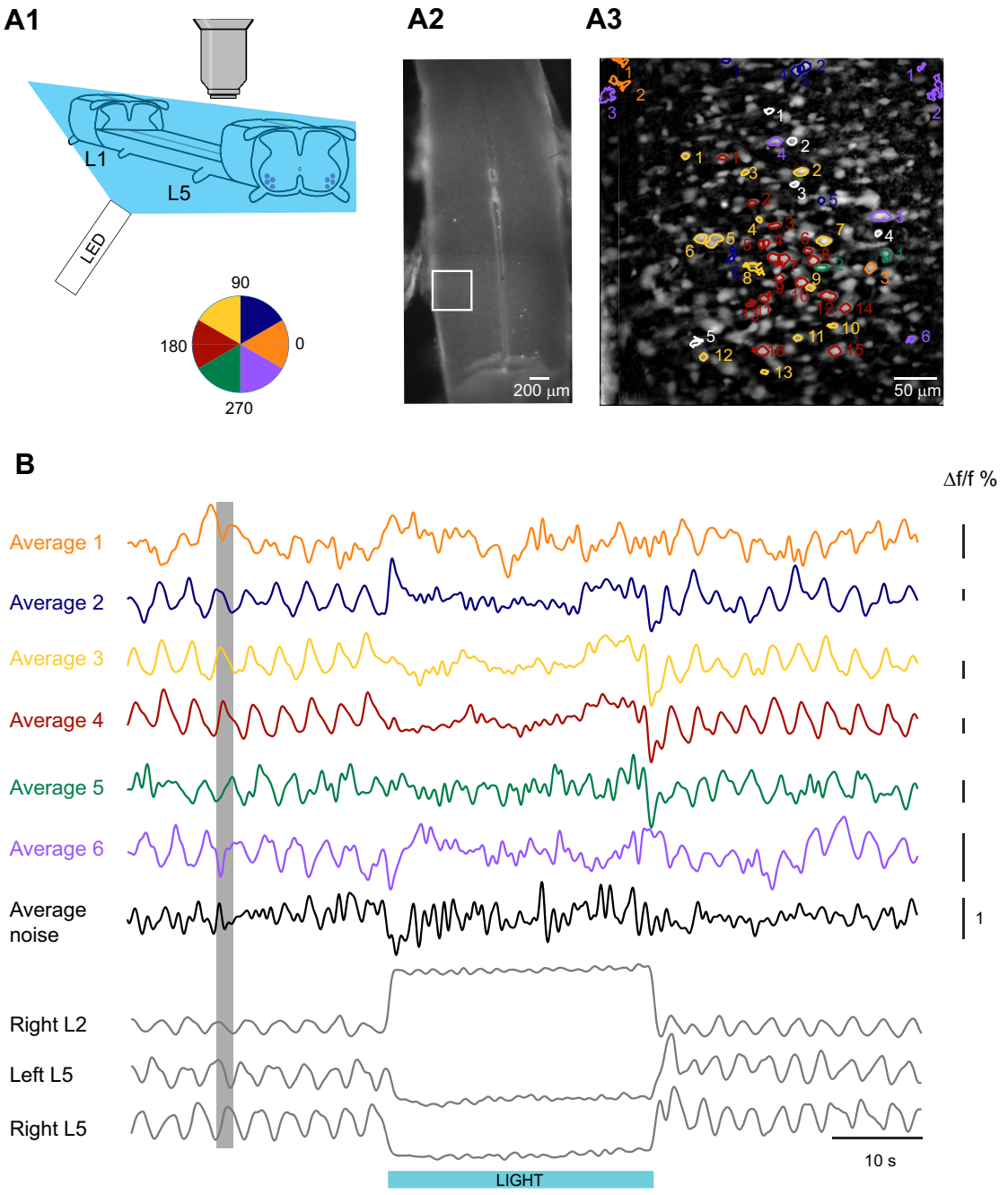

Figure 5. Depolarization of V1 interneurons disrupts rhythmic activity in all interneurons monitored with calcium imaging on dorsally shaved *En1*-ChR2 spinal cords. ***A1***, Schematic of the experimental setup, showing a drawing of an *En1*-ChR2 spinal cord that had its lumbar dorsal horn removed. Filled purple circles represent the MNs. The optical recordings were made from the cut surface. ***A2***, Low-magnification (4×) fluorescent picture (2 images were stitched together) showing the labeling of cells with fura-2 AM at the cut surface. White rectangle represents the FOV of a 20× objective and the approximate location of the recording. ***A3***, Representative fluorescent image of one of the recordings from a region of the left L5 segment as depicted in ***A2***. The ROIs identify small areas that were rhythmically active before the light and are color-coded according to their phasing as shown in the circular plot to the left. The white ROIs are examples of nonrhythmic ROIs. ***B***, Average recordings of all the ROIs separated according to their phasing together with the integrated neurograms from the right and left L5 and the right L2 ventral roots during locomotor-like activity induced with 5 μM NMDA, 10 μM 5-HT, and 50 μM DA. Blue bar represents the duration of the light.

the lumbar cord in the *En1*-ChR2 preparations, and bath-applied fura-2 AM to label the interneurons on the cut surface (Fig. 5*A*). fura-2 AM is excited by UV light, allowing us to excite the dye without activating either ChR2 or EYFP. We then induced locomotor-like activity with 5 μM NMDA, 10 μM 5-HT, and 50 μM DA. Before illumination, we observed cells or structures that were rhythmically active at different phases of the locomotor cycle compared with the left L5 ventral root recordings ($n = 7$ animals). We separated the phases into six groups and averaged the traces from each group (Fig. 5*B*). During illumination, in all recordings and in all groups, the averaged calcium signals followed the behavior of the VR recordings (either no rhythmic activity or a few isolated bursts). We found no evidence for interneurons that maintained the pre-light rhythm during the light, indicating that rhythmic calcium activity in interneurons is disrupted when V1 interneurons are depolarized. Of course, the limitation of this approach is that we cannot image the activity of all the interneurons in the ventral lumbar cord. Nevertheless, the

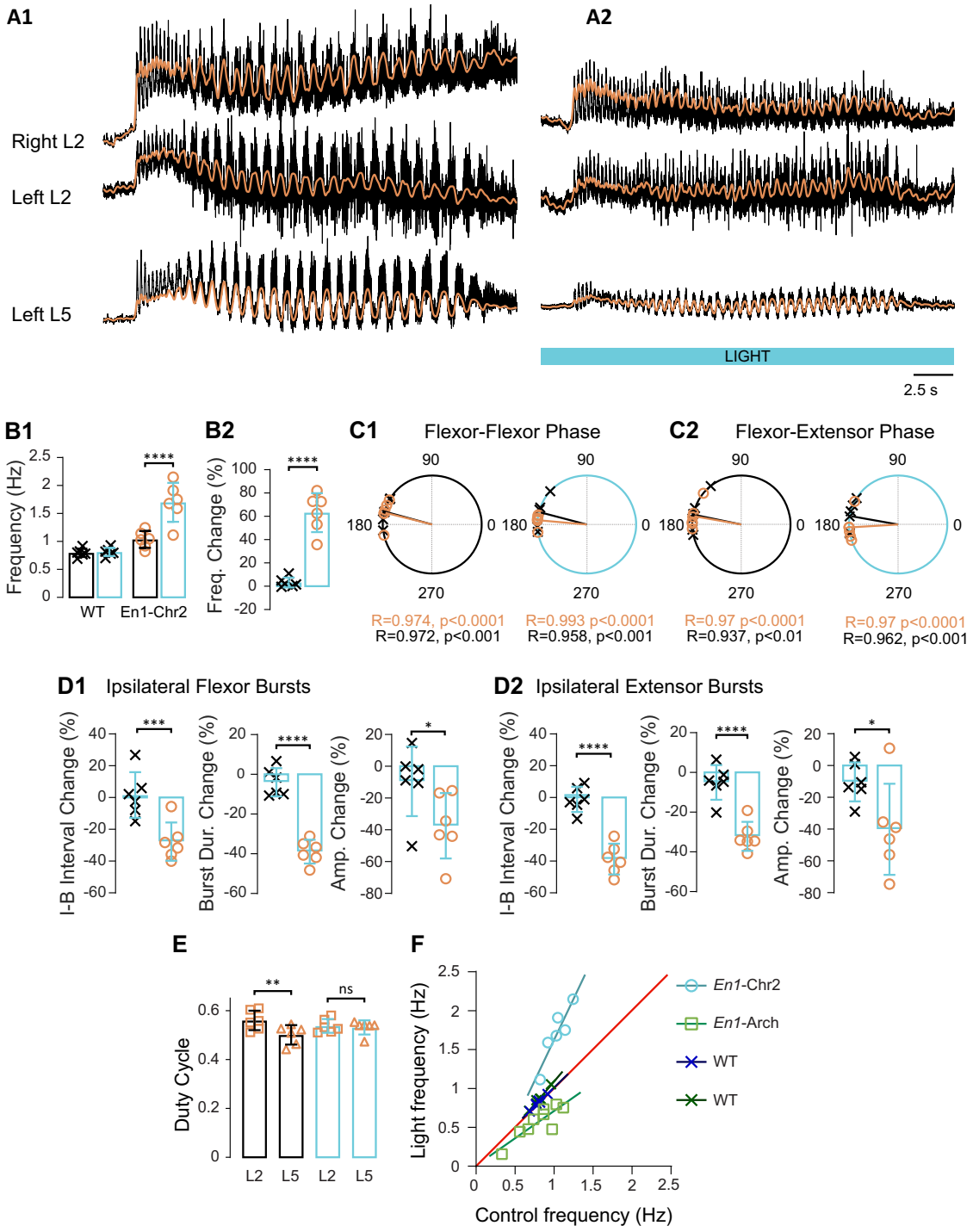

Figure 6. Depolarizing V1 interneurons accelerates the frequency of fictive locomotion evoked by brainstem stimulation in *En1*-ChR2 spinal cords. ***A***, Fictive locomotion evoked by brainstem stimulation before (***A1***) and during (***A2***) light-evoked depolarization of *En1*-postive neurons in an *En1*-ChR2 spinal cord. Locomotor-like activity was recorded from the right L2 and the left L2 and L5 ventral roots. Orange traces represent the slow potentials obtained by low-pass filtering of the raw neurograms. Blue bar below the recordings represents the duration of the light. ***B1***, Bar plots represent the frequency of the rhythm in the WT (black crosses, $n = 6$) and the *En1*-ChR2 (orange circles, $n = 6$) preparations before (black rectangles) and during illumination (blue rectangles); repeated-measures two-way ANOVA: light status, $F_{(1,10)} = 57.67$, $p < 0.0001$; genetic identity, $F_{(1,10)} = 29.07$, $p = 0.0003$; spinal cords, $F_{(10,10)} = 5.445$, $p = 0.0065$; interaction, $F_{(1,10)} = 52.49$, $p < 0.0001$. ***B2***, Bar plot represents the change (%) in frequency in WT (black crosses) and *En1*-ChR2 (orange circles) cords during illumination. *t* test, $p < 0.0001$. ***C***, Circular plots represent the phasing of the bilateral flexor (***C1***) and ipsilateral flexor-extensor (***C2***) ventral roots during fictive locomotion before (black circles) and during (blue circles) illumination of *En1*-ChR2 (orange circles) and WT (black crosses) spinal cords. *R* is the length of the vector, and *p* is the value for the Raleigh test of uniformity. Using the Harrison–Kaji test, we calculated the statistical difference between the two types of cords (genetic identity) and the difference before and during illumination (light status) for the phasing of the bilateral flexor and ipsilateral flexor-extensor ventral roots. The results of the test for the bilateral flexors were as follows: light status, $F_{(1,20)} = 0.68$, $p = 0.4206$; genetic identity, $F_{(1,20)} = 0.88$, $p = 0.3584$; interaction, $F_{(1,20)} = 0.55$, $p = 0.4681$. For the flexor-extensor phases, the results were as follows: light status, $F_{(1,20)} = 3.05$, $p = 0.0963$; genetic identity, $F_{(1,20)} = 1.24$, $p = 0.2785$; interaction, $F_{(1,20)} = 0.87$, $p = 0.3619$. ***D1***, Light-dependent changes in flexor ventral root bursts, ipsilateral to the recorded extensor ventral roots for *En1*-ChR2 (orange circles, $n = 6$) and WT (black crosses, $n = 6$) cords. Bar plots represent the changes (%) of the interburst (I-B) interval (left), burst duration (Dur; middle), and burst amplitude (Amp; right) during illumination (blue rectangle) compared with before the light. ***D2***, Similar measurements as for ***D1*** for the extensor ventral roots ipsilateral to the recorded flexor ventral roots. One-way ANOVA was used to statistically compare the

similarity of the behavior of the imaged interneurons with the ventral root recordings is consistent with the idea that V1 interneurons target the CPG and their depolarization disrupts rhythmic activity during drug-induced locomotor-like activity.

V1 neuron function during locomotor-like activity evoked by brainstem or sacral afferent stimulation

It is not clear that the networks responsible for locomotor-like activity evoked by electrical stimulation are identical to those engaged during drug-induced activity. Stimulus-evoked activity is generally faster than drug-induced fictive locomotion, and there are differences in the locomotor behavior evoked by the different neuronal sources (Whelan et al., 2000; Pujala et al., 2016). In addition, brainstem stimulation *in vivo* tends to produce a flexor-dominated rhythm, providing us with the opportunity to test whether V1 function was similar in all types of fictive locomotion. For these reasons, we examined the effects of activating V1 neurons on the locomotor-like activity evoked electrically by brainstem or by sacral dorsal root stimulation.

Brainstem stimulation

Brainstem stimulation in *En1*-ChR2 animals produced a flexor-biased locomotor-like rhythm in 5 of 6 experiments (Fig. 6) and in 3 of 6 experiments in WT preparations. Under control conditions, the frequency of the rhythm in *En1*-ChR2 cords was faster than that in the WT cords (1.04 ± 0.15 Hz, $n = 6$, vs 0.8 ± 0.07 Hz, $n = 6$ respectively, $p = 0.0366$). There were no significant, light-dependent changes in the frequency of the rhythm in WT spinal cords ($p = 0.082$, paired t test), whereas, surprisingly, V1 depolarization resulted in a statistically significant ($p = 0.0007$ paired t test; Fig. 6*A*,*B*) frequency increase (63.14 ± 16.7% over the pre-light frequency) that was also significantly higher than the light-dependent frequency change in WT cords (3.2 ± 4.2%; Welch's t test, $p = 0.0002$).

On exposure to light, the interburst intervals decreased in both the L2 and L5 ventral roots (L2: −27.75 ± 12.1, L5: −38.77 ± 9.7%, $n = 6$; Fig. 6*D*), with the largest effect in the L5 ventral root (paired t test, $p = 0.0097$). There was also a decrease in the L2 and L5 burst durations compared with WT (L2: −38.63 ± 6.1%, L5: −31.86 ± 7.5%). However, the difference between the L2 and L5 burst durations in the *En1*-ChR2 cords was not statistically different (paired t test $p = 0.0515$). There was little change in the duty cycles.

As with the drug-induced locomotion, depolarization of V1 interneurons induced a decrease in amplitude of the bursts in both the L2 and the L5 ventral roots compared with WT (−36.69 ± 20.98%, $p = 0.0425$; −40.11 ± 28.66%, $p = 0.0275$; $n = 6$, respectively). In 6 cords, locomotor-like activity was not evoked in the presence of the light. We hypothesized that, in these cords, the light was too intense and inhibited the CPG or its activation. In 4 of these cords, fictive locomotion was evoked by the brainstem stimulus when we reduced the intensity to 10% of the maximum, and its frequency was 19.83 ± 20% ($n = 4$) above the pre-light control, consistent with the light-dependent increase seen in the other experiments. However, because of the atypical nature of these results, we did not include them in the analysis.

We were surprised that the effect of V1 depolarization on the frequency of the rhythm evoked by brainstem stimulation was opposite than that seen during the drug-induced rhythms. Previous work showed that hyperpolarization of V1 interneurons slowed the rhythm in both drug-induced and dorsal root-evoked fictive locomotion (Falgairolle and O'Donovan, 2019). Accordingly, an acceleration of the rhythm would be predicted when the same neurons were depolarized, suggesting that the slowing observed during drug-induced rhythms was anomalous. To address this idea, we tested the effect of hyperpolarizing V1 neurons during brainstem-evoked rhythms in cords expressing archaerhodopsin in *En1* neurons. Brainstem stimulation in these preparations also produced flexor-biased fictive locomotion ($n = 9$ of 9). We found that hyperpolarizing V1 interneurons during brainstem-evoked locomotor-like activity led to a decrease in frequency (−29.61 ± 13.74%) that was statistically different from control (6.92 ± 2.15%). This was because of an increase of the interburst interval (L2: 34.38 ± 41.62, L5: 59.90 ± 61.50) as well as an increase in the burst duration of both the flexor and extensor ventral roots (L2: 60.76 ± 54.47%, L5: 51.92 ± 54.47%), and these changes were statistically different from the effects observed in the WT spinal cords. For both the *En1*-ChR2 and the *En1*-Arch cords, the light-dependent changes in frequency were proportional to the initial frequency, with the largest changes (increases for *En1*-Chr2 and decreases for *En1*-Arch) occurring at the highest initial frequencies (Fig. 6*F*). This dependence was not seen in the WT preparations.

The phasing in the *En1*-Arch changed slightly during hyperpolarization between the ipsilateral flexor/extensor ventral roots. We did not find any statistically significant changes in the amplitude of the bursts. These findings suggest that it is not brainstem stimulation per se that accounts for the opposing directions of the light-induced frequency change seen in brainstem- and drug-evoked fictive locomotion in the *En1*-ChR2 cords, and that some aspect of the drug-induced rhythms is responsible.

Sacral dorsal root stimulation

In the last set of experiments, we examined the effects of depolarizing V1 interneurons during locomotor-like activity evoked by stimulation of sacral dorsal roots.

In contrast to both the drug cocktail and brainstem stimulation, we found that V1 depolarization during locomotor-like activity evoked by sacrocaudal stimulation, did not change the frequency of fictive locomotion (7.39 ± 15.53%, from 1.1 ± 0.11 Hz to 1.15 ± 0.19 Hz; Fig. 7*A*,*B*) compared with the effect of light in the control *En1*-GFP spinal cords (−0.33 ± 1.37%, from 0.91 ± 0.1 Hz to 0.91 ± 0.11 Hz). In *En1*-ChR2 cords, the burst duration (L2: −10.49 ± 17.43%, L5 0.91 ± 20.07%; Fig. 7*D*) and interburst intervals (L2: −3.594 ± 17.62%, L5: −11.23 ± 28.93%; Fig. 7*D*) and the

←

I-B interval, burst duration, and amplitude change between flexor and extensor ventral roots in *En1*-ChR2 and WT preparations during illumination. I-B interval, $F_{(3,20)} = 18.59$, $p < 0.0001$; burst duration, $F_{(3,20)} = 35.12$, $p < 0.0001$; amplitude, $F_{(3,20)} = 3.467$, $p = 0.0356$. ***E***, Duty cycle of the flexor (L2, orange squares) and the extensor (L5, orange triangles) cycles in *En1*-ChR2 spinal cords before (black rectangles) and during illumination (repeated-measures two-way ANOVA: light status, $F_{(1,5)} = 0.1603$, $p = 0.7054$; root identity, $F_{(1,5)} = 2.251$, $p = 0.1939$; interaction, $F_{(1,5)} = 11.77$, $p = 0.0186$). ***F***, Plot represents the frequency of the rhythm before the light (control frequency) plotted against the frequency of the rhythm during the light (light frequency) in *En1*-ChR2 (blue circles), *En1*-Arch (green squares), WT illuminated with blue light (dark blue crosses), and WT illuminated with green light (dark green crosses) cords. Red line indicates the line of unity where the frequency is the same before and during light. Blue and green lines indicate the linear regressions calculated for the experiments with the darker lines calculated for the WT experiments. WT blue light ($n = 6$; Pearson correlation $r = 0.972$, $p = 0.0012$, slope: 0.9651x + 0.0434); WT green light ($n = 6$; Pearson correlation $r = 0.9862$, $p = 0.0003$, slope: 1.179x − 0.08912); *En1*-ChR2 ($n = 6$; Pearson correlation $r = 0.9137$, $p = 0.0108$, slope: 2.103x − 0.4787); and *En1*-Arch ($n = 9$; Pearson correlation $r = 0.8612$, $p = 0.0029$, slope: 0.7023x + 0.007805). *$p < 0.05$. **$p < 0.01$. ***$p < 0.001$. ****$p < 0.0001$.

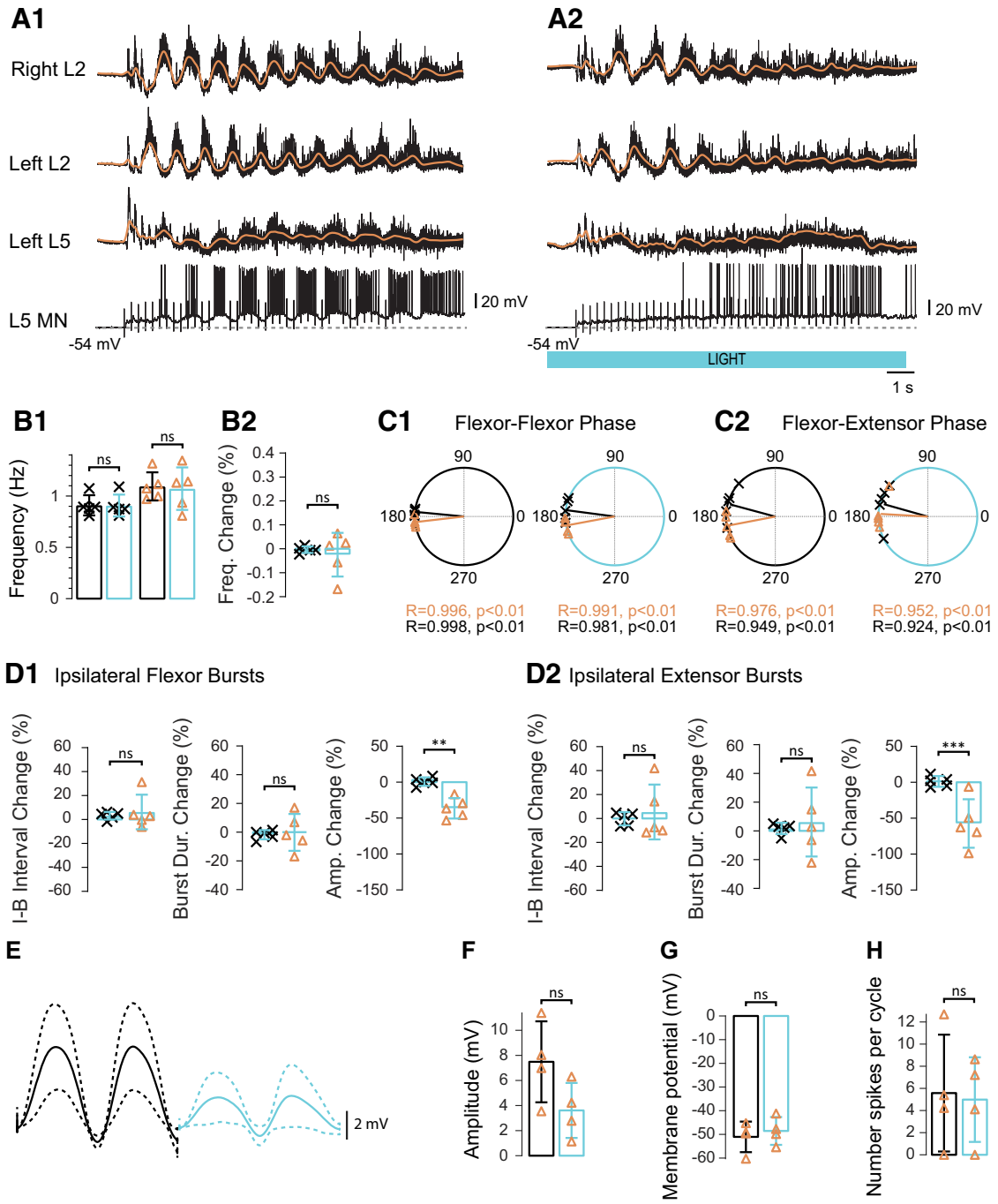

Figure 7. Depolarizing V1 interneurons does not significantly change the frequency of fictive locomotion evoked by sacrocaudal afferent stimulation in *En1*-ChR2 spinal cords. ***A***, Fictive locomotion evoked by stimulating a sacral dorsal root before (***A1***) and during (***A2***) light depolarization of V1 neurons in an *En1*-ChR2 spinal cord. Locomotor-like activity was recorded from the right L2 and the left L2 and L5 together with an intracellular recording of an extensor MN. Orange traces represent the slow potentials obtained by low-pass filtering of the raw neurograms. Blue bar below the recordings represents the duration of the light. ***B1***, Bar plots represent the frequency of the rhythm in the *En1*-GFP (black crosses, $n = 5$) and the *En1*-ChR2 (orange circles, $n = 8$) preparations before (black rectangles) and during illumination (blue rectangles), repeated-measures two-way ANOVA: light status, $F_{(1,11)} = 1.107$, $p = 0.3152$; genetic identity, $F_{(1,11)} = 8.194$, $p = 0.0154$; spinal cords, $F_{(11,11)} = 3.974$, $p = 0.0155$; interaction, $F_{(1,1)} = 1.268$, $p = 0.2841$. ***B2***, Bar plot represents the change (%) in frequency in WT (black crosses) and *En1*-ChR2 (orange triangles) during illumination. *t* test, $p = 0.2987$. ***C***, Circular plots represent the phasing of the bilateral flexor (***C1***) and ipsilateral flexor-extensor (***C2***) ventral roots during fictive locomotion before (black circles) and during (blue circles) illumination of *En1*-ChR2 (orange triangles) and *En1*-GFP (black crosses) spinal cords. *R* is the length of the vector, and *p* is the value for the Raleigh test of uniformity. Using the Harrison–Kaji test, we calculated the statistical difference between the two types of cord (genetic identity) and the difference before and during illumination (light status) for the phasing in bilateral flexor and ipsilateral flexor-extensor ventral roots. The result of the test for the bilateral flexor was as follows: light status, $F_{(1,22)} = 0.22$, $p = 0.6463$; genetic identity, $F_{(1,22)} = 15.71$, $p = 0.0007$; interaction, $F_{(1,22)} = 0.59$, $p = 0.45$. We then performed a Watson–Williams test to compare the *En1*-ChR2 and the *En1*-GFP bilateral flexor phasing before and during illumination ($F_{(1,11)} = 15.63$, $p = 0.0023$; and $F_{(1,11)} = 6.79$, $p = 0.0245$; respectively). For the flexor-extensor phases, the results were as follows: light status, $F_{(1,22)} = 4.11$, $p = 0.0549$; genetic identity, $F_{(1,22)} = 2.75$, $p = 0.1116$; interaction, $F_{(1,22)} = 0.17$, $p = 0.6808$. ***D1***, Light-dependent changes in flexor ventral root bursts, ipsilateral to the recorded extensor ventral root for *En1*-ChR2 (orange triangles) and *En1*-GFP (black crosses) cords. Bar plots represent the changes (%) of the interburst (I-B) interval (left), burst duration (Dur; middle), and burst amplitude (Amp; right) during illumination (blue rectangle) compared with before the light. ***D2***, Similar measurements as for ***D1*** for the extensor ventral roots ipsilateral to the recorded flexor ventral roots. One-way ANOVA was used to statistically compare the I-B interval, burst duration, and amplitude change between flexor and extensor dominated ventral roots in *En1*-ChR2 and *En1*-GFP preparations during illumination. I-B interval: $F_{(3,22)} = 0.6698$, $p = 0.5796$; burst duration, $F_{(3,22)} = 1.006$, $p = 0.4090$; amplitude, $F_{(3,22)} = 16.29$, $p < 0.0001$. ***E***,

phasing (Fig. 7*C*) did not change significantly during illumination compared with the control *En1*-GFP cords; as a result, the duty cycle did not vary significantly. However, there was a decrease in the burst amplitudes (Fig. 7*D*) in both the L2 and the L5 ventral roots (L2: $-37.44 \pm 13.1\%$, L5: $-54.08 \pm 26.71\%$). We also performed intracellular recordings of MNs, all of which were in spinal cords exhibiting extensor-biased locomotor-like activity ($n = 4$). We found no statistically significant differences for the membrane potential or the number of spikes per cycles in the recorded MNs (Fig. 7*G*,*H*). However, the amplitude of the synaptic drive was smaller during the light, although this did not reach statistical significance (from 7.49 ± 3.23 mV to 3.61 ± 2.2 mV; Fig. 7*E*,*F*).

The rhythm produced by sacral dorsal root stimulation was either flexor (3 of 7 cords) or extensor biased (4 of 7 cords) in the *En1*-Chr2 cords, and largely extensor-biased (4 of 5 cords) in the control *En1*-GFP spinal cords. On separating the effects of light in the extensor- and flexor- biased *En1*-ChR2 cords, we found that depolarization of V1 interneurons did not change the frequency ($-2.46 \pm 9.13\%$) during extensor-biased fictive locomotion, whereas it increased it ($23.79 \pm 5.56\%$) during flexor-biased fictive locomotion (Fig. 8). These differences were statistically significant (one-way ANOVA, $p = 0.0048$). In the flexor-biased cords, there was also a change in the L2 burst duration and interburst interval and in the L5 interburst interval.

Discussion

We found that the effects of depolarizing V1 interneurons are more complex than previously demonstrated and depend on how the rhythm was activated. V1 depolarization slowed and disrupted the drug-induced rhythm in whole cords but slowed it in hemicords. However, during stimulus-evoked fictive locomotion, the effects of V1 depolarization depended on the source of the stimulus. V1 depolarization accelerated the frequency during brainstem stimulation and was without effect during sacral dorsal root stimulation. For both drug-induced and brainstem-evoked locomotor-like activity, the change in frequency was dependent on the initial frequency of the rhythm, an effect that may be linked to the progressive recruitment of V1 interneurons as the locomotor frequency increases. Collectively, these results indicate that the functional action of the V1 population is not fixed but depends on the state of the locomotor network.

V1 interneurons target the CPG and regulate the locomotor frequency

Ablation or hyperpolarization of V1s decreases the frequency of locomotion in both zebrafish and mice (Gosgnach et al., 2006; Britz et al., 2015; Falgairolle and O'Donovan, 2019; Kimura and Higashijima, 2019), suggesting that V1 neurons target the locomotor CPG. We provided two additional lines of evidence in support of this conclusion. First, we demonstrated that brief optical activation of V1s resets the locomotor rhythm, and second by showing that all rhythmically active MNs and interneurons are silenced, or show disrupted activity, when V1 interneurons are depolarized during drug-induced fictive locomotion. This latter result suggests that the V1 activation can silence the rhythm generator, with the caveat that our imaging only captures the activity of interneurons on the cut surface of the cord.

During locomotion evoked by brainstem stimulation, V1 depolarization accelerated the rhythm. To account for this result, we consider the computational model of Shevtsova and Rybak (2016), who proposed the existence of two V1 types within the locomotor rhythm generator. One is normally activated by contralateral input (here designated V1c) and inhibits the extensor half-center as well as a non-V1 inhibitory interneuron that inhibits the flexor center, whereas the other (V1-1) is driven by extensor half-center and inhibits the flexor half-center (Fig. 9). According to the model, these two inhibitory neuron classes regulate the speed of locomotion by inhibiting or disinhibiting the flexor half-center (see also Falgairolle and O'Donovan, 2019). To explain the V1-induced acceleration of the rhythm, we propose that the activity of the V1s receiving excitation from the extensor half-center (V1-1) is relatively weaker than the V1c interneurons that are driven contralaterally, either because fewer V1-1 neurons are recruited during locomotion evoked by brainstem stimulation or because they are driven less effectively by the extensor half-center. When both V1 classes are depolarized, the dominant effect will be to accelerate the rhythm because the V1c neurons inhibit both the extensor half-center and the non-V1 neurons projecting to the flexor half-center, thereby disinhibiting the flexor center and causing the rhythm to accelerate. Accounting for the effects of V1 depolarization on drug-induced fictive locomotion or fictive locomotion evoked by stimulation of sacrocaudal afferents is more challenging because the effects differ according to how the rhythm is activated. V1 depolarization slows the rhythm in drug-induced locomotion and produces little or no change in the frequency during dorsal root stimulation. Therefore, to explain these effects, we must assume that the different modes of stimulation differentially recruit the V1-1 and the V1c populations. Confirmation of these ideas will require the development of methods to selectively label and monitor the two V1 populations.

By removing contralateral inputs, hemisections provide a simplified network in which to examine the function of V1s. One limitation of the preparation is that, while the drug cocktail produces organized (flexor-extensor) rhythmic activity in the hemicords, electrical stimulation of afferents produces only tonic activity (data not shown). Depolarizing V1 interneurons in hemicords during ongoing rhythmic activity slowed the rhythm, consistent with the previously reported acceleration caused by V1 hyperpolarization (Falgairolle and O'Donovan, 2019). In the earlier work, the results were accounted for by arguing that the V1c neurons normally receiving tonic contralateral excitation are silent in the hemicord, which removes the inhibition of both the extensor half-center and the non-V1 neurons projecting to the flexor half-center, resulting in a slower rhythm in the hemicord (Fig. 9). When the V1-1 neuron is hyperpolarized, this interrupts the inhibitory drive originating from the extensor half-center, thereby accelerating the rhythm. Conversely, when V1s are depolarized, as in the present work, the V1-1 neuron projecting to the flexor center is now activated more intensely, which slows the rhythm. We also observed a decrease of the flexor and an increase of the extensor duty cycles. As V1s have more terminals on flexor MNs, their activation could lead to a shortening of the flexor bursts with a corresponding increase of the interburst intervals, accompanied by an increase in the duration of the extensor MN bursts (Falgairolle and O'Donovan, 2019).

←

Cycle-triggered average (continuous line, 2 cycles) and SD (dotted lines) of a synaptic drive to an MN during fictive locomotion evoked by stimulating sacrocaudal afferents ($n = 4$) in *En1*-ChR2 spinal cords before (black) and during (blue) illumination. ***F***, Bar plot represents the amplitude of the synaptic drive (*t* test, $p = 0.1069$). ***G***, Bar plot represents the membrane potential (*t* test, $p = 0.1243$). ***H***, Bar plot represents the number of spikes per cycle (*t* test, $p = 0.6667$). $^{**}p < 0.01$. $^{***}p < 0.001$.

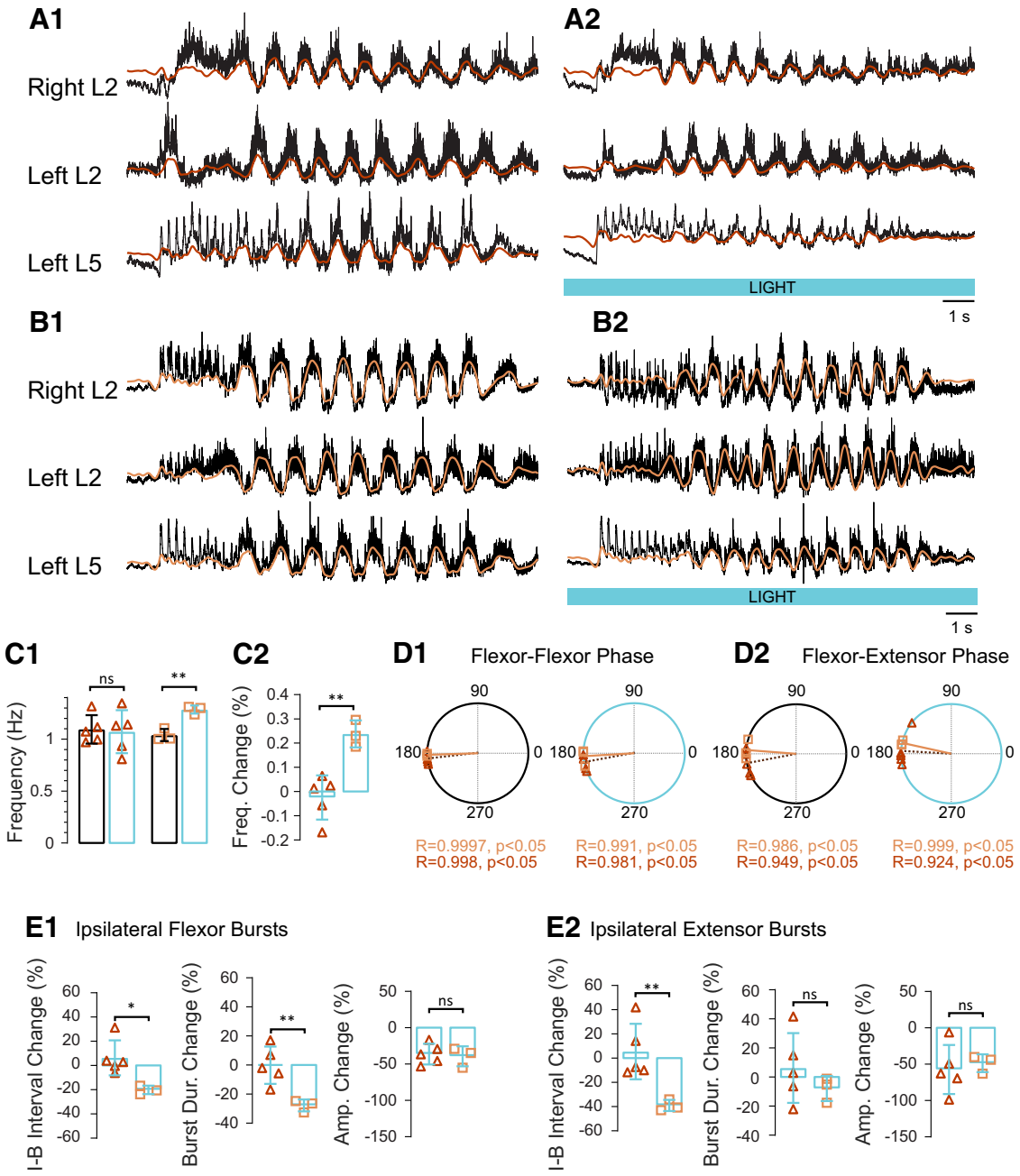

Figure 8. Depolarizing V1 interneurons increases the frequency of flexor-biased fictive locomotion evoked by sacrocaudal afferent stimulation in En1-ChR2 spinal cords. Extensor-biased fictive locomotion evoked by stimulating a sacral dorsal root before (***A1***) and during (***A2***) light-induced depolarization of En1-postive neurons in an En1-ChR2 spinal cord. Locomotor-like activity was recorded from the right L2 and the left L2 and L5 ventral roots. Red traces represent the slow potentials obtained by low-pass filtering of the raw signals. Blue bar below the recordings represents the duration of the light. ***B***, Flexor-biased fictive locomotion evoked by stimulating a sacral dorsal root before (***B1***) and during (***B2***) light-induced depolarization of En1-postive neurons in an En1-ChR2 spinal cord. Locomotor-like activity was recorded from the right L2 and the left L2 and L5 ventral roots. Orange traces represent the slow potentials obtained by low-pass filtering of the raw signals. Blue bar below the recordings represents the duration of the light. ***C1***, Bar plot represents the frequency of the rhythm in the extensor-biased En1-ChR2 (red triangles, $n = 5$) and the flexor-biased En1-ChR2 (orange squares, $n = 3$) preparations before (black rectangles) and during illumination (blue rectangles), repeated-measures two-way ANOVA, light status: $F_{(1,6)} = 14.68$, $p = 0.0086$; genetic identity: $F_{(1,6)} = 0.598$, $p = 0.4687$; spinal cords: $F_{(6,6)} = 12.46$, $p = 0.0307$; interaction: $F_{(1,6)} = 21.21$, $p = 0.0037$. ***C2***, Bar plot represents the change (%) in frequency in extensor-biased and flexor-biased fictive locomotion in En1-ChR2 spinal cords (red triangles and orange squares, respectively) during illumination. *t* test, $p = 0.0044$. ***D***, Circular plots represent the phasing of the bilateral flexor (***D1***) and ipsilateral flexor-extensor (***D2***) ventral roots before (black circles) and during (blue circles) illumination of extensor-biased fictive locomotion (red triangles) and flexor-biased locomotion (orange squares) in En1-ChR2 spinal cords. *R* is the length of the vector, and *p* is the value for the Raleigh test of uniformity. Using the Harrison–Kaji test, we calculated the statistical difference between the two types of cord (genetic identity) and the differences before and during illumination (light status) for the phasing in bilateral flexor and ipsilateral flexor-extensor ventral roots. The result of the test for the bilateral flexor was as follows: light status, $F_{(1,12)} = 0.8$, $p = 0.3898$; genetic identity, $F_{(1,12)} = 2.82$, $p = 0.1188$; interaction, $F_{(1,12)} = 0.11$, $p = 0.7412$. For the flexor-extensor phases, the results was as follows: light status, $F_{(1,12)} = 3.87$, $p = 0.0726$; genetic identity, $F_{(1,12)} = 1.18$, $p = 0.2629$; interaction, $F_{(1,12)} = 0.14$, $p = 0.7102$. ***E1***, Light-dependent changes in flexor ventral root bursts, ipsilateral to the recorded extensor ventral root for extensor-biased fictive locomotion in En1-ChR2 (red triangles) and in flexor-biased locomotion in En1-ChR2 (orange squares) cords. Bar plots represent the changes (%) of the interburst (I-B) interval (left), burst duration (Dur; middle), and burst amplitude (Amp; right) during illumination (blue rectangle) compared with before the light. ***E2***, Similar measurements as for ***E1*** for the extensor ventral roots ipsilateral to the

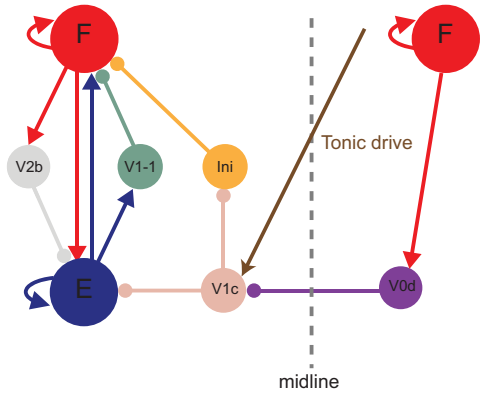

Figure 9. Simplified model of how V1 interneurons might regulate the CPG. Schematic showing putative connections of V1 interneurons with the rhythmogenic circuitry on one side of the cord. It consists of an extensor (E) and a flexor (F) center, mutually inhibiting each other via V2b or V1-1 interneurons. V1c interneurons receive contralateral excitation and inhibition from the V0d interneurons, and inhibit both the extensor center and Ini, an undefined inhibitory population, that inhibits the flexor center. Contralateral V0d interneurons receive inputs from the contralateral flexor center. Modified from Shevtsova and Rybak (2016).

In the zebrafish, V1 interneurons are comprised of two classes (fast and slow) that have selective projections to excitatory V2a interneurons and to MNs (Kimura and Higashijima, 2019). The V2as are connected to MNs in three distinct modules that are active in slow, intermediate, and fast swimming. Slow V1s are active in slow swimming and project to slow V2as and to slow MNs. The fast V1s are active in fast swimming and project to both the slow and fast swimming modules. Locomotor speed control by V1 neurons is thus accomplished in two ways. First, the slow and fast V1s regulate the termination of the bursts in slow and fast MNs, respectively, and the fast have an additional function of inhibiting the slow V2a/MN module during fast swimming (Kimura and Higashijima, 2019). In mammalian locomotion, spinal modules also control locomotor speed and gait, particularly those including V0 and V2a neurons (Crone et al., 2009; Zhong et al., 2010; Talpalar et al., 2013; Bellardita and Kiehn, 2015). Whether V1s can control the function of these modules is not known, but such an action could contribute to the regulation of locomotor speed. While V1s in the zebrafish are recruited according to swimming speed, it is not known whether a similar pattern of recruitment occurs in mammals. Our evidence suggests that more and/or different subsets of V1 interneurons are recruited as locomotor speed increases because the frequency change of the rhythm produced by V1 depolarization was proportional to the pre-light locomotor frequency. Larger light-dependent changes would be expected if more V1 interneurons were available to be modulated by the light at the higher speeds (Falgairolle and O'Donovan, 2019).

Interestingly, in the whole cord, the light-dependent decrease in frequency was transient; whereas in the hemicord, it was maintained for the duration of the light. The persistence of the frequency change in the hemicord indicates that the functional effect of V1 depolarization can last up to 60 s, indicating that the V1 interneurons do not experience depolarization block. Depolarization block would mimic the effect of V1 hyperpolarization leading to a frequency increase: the opposite of what was observed.

Table 1. Summary of the effects of light on the frequency of the locomotor rhythm during activation by different methods and according to the flexor-extensor bias of the evoked rhythm

Activation Source	Bias	Frequency
Brainstem	Flexor	Increase
	Extensor	Increase
Afferents	Flexor	Increase
	Extensor	No change
Drugs	Flexor	Increase
	Extensor	Decrease

V1 depolarization effects in flexor- and extensor-biased rhythms

We found that fictive locomotion evoked by drug cocktail or dorsal root stimulation tended to produce extensor-biased fictive locomotion, as was observed in a previous study (Falgairolle and O'Donovan, 2019), whereas brainstem stimulation generally produced flexor-biased fictive locomotion. When we separated the preparations that exhibited flexor-biased fictive locomotion, all showed an increase in frequency during V1 depolarization regardless of their mode of activation. However, preparations with extensor-biased fictive locomotion exhibited different behaviors depending on the mode of activation. For example, in extensor-biased fictive locomotion triggered by sacrocaudal afferent stimulation, there was no systematic effect of light on the rhythm, whereas the rhythm accelerated in sacrocaudal afferent-induced, flexor-biased fictive locomotion. These results are summarized in Table 1, which shows the effect of light on the frequency of the rhythm according to the mode of activation and whether the evoked rhythm was flexor- or extensor-biased. These data show that the initial state of the network, extensor- or flexor-biased, also influences the functional actions of V1s.

In summary, the diverse actions of V1 interneurons during fictive locomotion evoked by different methods suggest the operation of functionally distinct neuronal circuits. However, the relationship of the different modes of activation we have used *in vitro* to the initiation and maintenance of naturally occurring locomotion is not known. In intact animals, locomotion can be triggered or facilitated in several ways, including drugs (clonidine or L-DOPA) (Forssberg and Grillner, 1973; Britz et al., 2015), perineal stimulation (Barbeau and Rossignol, 1987; Merlet et al., 2021), or epidural stimulation (Gerasimenko et al., 2008). Ultimately, it will be necessary to study V1 function under these different modes of excitation to establish whether a similar multifunctionality of V1 neurons is present *in vivo*.

Nevertheless, our results add to a growing body of evidence that supports the idea of greater flexibility in the organization and recruitment of networks producing locomotion (Pham et al., 2020; Rancic et al., 2020) than previously believed. Furthermore, they raise the possibility that other neuronal classes, defined by transcription expression, may have variable functional roles according to how they are recruited during locomotion.

←

recorded flexor ventral roots. One-way ANOVA was used to statistically compare the I-B interval, burst duration, and amplitude change between flexor- and extensor-biased ventral roots in both preparations during illumination. I-B interval, $F_{(3,12)} = 6.988$, $p = 0.0057$; burst duration, $F_{(3,12)} = 2.966$, $p = 0.0747$; amplitude, $F_{(3,12)} = 0.8359$, $p = 0.4997$. *$p < 0.05$. **$p < 0.01$.

References

Antri M, Mellen N, Cazalets JR (2011) Functional organization of locomotor interneurons in the ventral lumbar spinal cord of the newborn rat. PLoS One 6:e20529.

Ayers JL, Selverston AI (1979) Mono-synaptic entrainment of an endogenous pacemaker network-cellular mechanism for Vonholsts magnet effect. J Comp Physiol 129:5–17.

Barbeau H, Rossignol S (1987) Recovery of locomotion after chronic spinalization in the adult cat. Brain Res 412:84–95.

Bellardita C, Kiehn O (2015) Phenotypic characterization of speed-associated gait changes in mice reveals modular organization of locomotor networks. Curr Biol 25:1426–1436.

Berens P (2009) CircStat: a MATLAB toolbox for circular statistics. J Stat Softw 31:1–21.

Bikoff JB, Gabitto MI, Rivard AF, Drobac E, Machado TA, Miri A, Brenner-Morton S, Famojure E, Diaz C, Alvarez FJ, Mentis GZ, Jessell TM (2016) Spinal inhibitory interneuron diversity delineates variant motor microcircuits. Cell 165:207–219.

Bracci E, Ballerini L, Nistri A (1996) Localization of rhythmogenic networks responsible for spontaneous bursts induced by strychnine and bicuculline in the rat isolated spinal cord. J Neurosci 16:7063–7076.

Britz O, Zhang J, Grossmann KS, Dyck J, Kim JC, Dymecki S, Gosgnach S, Goulding M (2015) A genetically defined asymmetry underlies the inhibitory control of flexor-extensor locomotor movements. Elife 4:e13038.

Crone SA, Zhong G, Harris-Warrick R, Sharma K (2009) In mice lacking V2a interneurons, gait depends on speed of locomotion. J Neurosci 29:7098–7109.

Duysens J (1977) Fluctuations in sensitivity to rhythm resetting effects during the cat's step cycle. Brain Res 133:190–195.

Falgairolle M, O'Donovan MJ (2019) V1 interneurons regulate the pattern and frequency of locomotor-like activity in the neonatal mouse spinal cord. PLoS Biol 17:e3000447.

Falgairolle M, Puhl JG, Pujala A, Liu W, O'Donovan MJ (2017) Motoneurons regulate the central pattern generator during drug-induced locomotor-like activity in the neonatal mouse. eLife 6:e26622.

Forssberg H, Grillner S (1973) The locomotion of the acute spinal cat injected with clonidine i.v. Brain Res 50:184–186.

Frigon A, Gossard JP (2009) Asymmetric control of cycle period by the spinal locomotor rhythm generator in the adult cat. J Physiol 587:4617–4628.

Gerasimenko Y, Roy RR, Edgerton VR (2008) Epidural stimulation: comparison of the spinal circuits that generate and control locomotion in rats, cats and humans. Exp Neurol 209:417–425.

Gosgnach S, Lanuza GM, Butt SJ, Saueressig H, Zhang Y, Velasquez T, Riethmacher D, Callaway EM, Kiehn O, Goulding M (2006) V1 spinal neurons regulate the speed of vertebrate locomotor outputs. Nature 440:215–219.

Kimura Y, Higashijima SI (2019) Regulation of locomotor speed and selection of active sets of neurons by V1 neurons. Nat Commun 10:2268.

Kwan AC, Dietz SB, Zhong G, Harris-Warrick RM, Webb WW (2010) Spatiotemporal dynamics of rhythmic spinal interneurons measured with two-photon calcium imaging and coherence analysis. J Neurophysiol 104:3323–3333.

McClellan AD, Jang W (1993) Mechanosensory inputs to the central pattern generators for locomotion in the lamprey spinal cord: resetting, entrainment, and computer modeling. J Neurophysiol 70:2442–2454.

Mentis GZ, Alvarez FJ, Bonnot A, Richards DS, Gonzalez-Forero D, Zerda R, O'Donovan MJ (2005) Noncholinergic excitatory actions of motoneurons in the neonatal mammalian spinal cord. Proc Natl Acad Sci USA 102:7344–7349.

Merlet AN, Harnie J, Macovei M, Doelman A, Gaudreault N, Frigon A (2021) Cutaneous inputs from perineal region facilitate spinal locomotor activity and modulate cutaneous reflexes from the foot in spinal cats. J Neurosci Res 99:1448–1473.

Mor Y, Lev-Tov A (2007) Analysis of rhythmic patterns produced by spinal neural networks. J Neurophysiol 98:2807–2817.

Pham BN, Luo J, Anand H, Kola O, Salcedo P, Nguyen C, Gaunt S, Zhong H, Garfinkel A, Tillakaratne N, Edgerton VR (2020) Redundancy and multifunctionality among spinal locomotor networks. J Neurophysiol 124:1469–1479.

Preibisch S, Saalfeld S, Schindelin J, Tomancak P (2010) Software for bead-based registration of selective plane illumination microscopy data. Nat Methods 7:418–419.

Pujala A, Blivis D, O'Donovan MJ (2016) Interactions between dorsal and ventral root stimulation on the generation of locomotor-like activity in the neonatal mouse spinal cord. eNeuro 3:ENEURO.0101-16.2016.

Rancic V, Ballanyi K, Gosgnach S (2020) Mapping the dynamic recruitment of spinal neurons during fictive locomotion. J Neurosci 40:9692–9700.

Schindelin J, Arganda-Carreras I, Frise E, Kaynig V, Longair M, Pietzsch T, Preibisch S, Rueden C, Saalfeld S, Schmid B, Tinevez JY, White DJ, Hartenstein V, Eliceiri K, Tomancak P, Cardona A (2012) Fiji: an open-source platform for biological-image analysis. Nat Methods 9:676–682.

Shevtsova NA, Rybak IA (2016) Organization of flexor-extensor interactions in the mammalian spinal cord: insights from computational modelling. J Physiol 594:6117–6131.

Sweeney LB, Bikoff JB, Gabitto MI, Brenner-Morton S, Baek M, Yang JH, Tabak EG, Dasen JS, Kintner CR, Jessell TM (2018) Origin and segmental diversity of spinal inhibitory interneurons. Neuron 97:341–355.e343.

Talpalar AE, Bouvier J, Borgius L, Fortin G, Pierani A, Kiehn O (2013) Dual-mode operation of neuronal networks involved in left-right alternation. Nature 500:85–88.

Whelan P, Bonnot A, O'Donovan MJ (2000) Properties of rhythmic activity generated by the isolated spinal cord of the neonatal mouse. J Neurophysiol 84:2821–2833.

Winfree AT (1975) Resetting biological clocks. Physics Today 28:34–39.

Yakovenko S, McCrea DA, Stecina K, Prochazka A (2005) Control of locomotor cycle durations. J Neurophysiol 94:1057–1065.

Zaporozhets E, Cowley KC, Schmidt BJ (2004) A reliable technique for the induction of locomotor-like activity in the in vitro neonatal rat spinal cord using brainstem electrical stimulation. J Neurosci Methods 139:33–41.

Zhong G, Droho S, Crone SA, Dietz S, Kwan AC, Webb WW, Sharma K, Harris-Warrick RM (2010) Electrophysiological characterization of V2a interneurons and their locomotor-related activity in the neonatal mouse spinal cord. J Neurosci 30:170–182.